EXPERIMENT AND NUMERICAL MODELING OF ROCK MOUND TO REDUCE WAVE OVERWASH AND CREST LOWERING OF A SAND BARRIER

BY

TINGTING ZHU AND NOBUHISA KOBAYASHI

RESEARCH REPORT NO. CACR-21-01
SPRING 2021

CENTER FOR APPLIED COASTAL RESEARCH

University of Delaware
Newark, Delaware 19716

ACKNOWLEDGMENTS

This study was supported by the U.S. Army Corps of Engineers under Agreement No. W912HZ18P0134 and by the U.S. Coastal Research Program under Agreement No. W912HZ20-2-0016.

TABLE OF CONTENTS

LIST OF TABLES

LIST OF FIGURES

ABSTRACT

Irregular wave overwash may cause landward migration and crest lowering of barrier beaches during a storm. Rock structures may protect barrier beaches but available data are very limited. Wave overwash process on barrier beaches without and with a structure has not been measured during a storm because of field work difficulty. Three hydraulic model tests were conducted in a small-scale experiment to investigate wave overwash and erosion process of a narrow sand barrier with no structure, a rock mound, and a rock cover. The rock mound consisting of three layers of stable stones reduced the landward migration and crest lowering of the sand barrier but sand transport through the porous structure was appreciable. The rock cover consisting of a single layer of stable stones was not effective in reducing the barrier deformation because of the stone settlement and spreading which resulted in the exposure of underlying sand to direct wave action. The exposed sand among the stones was eroded and transported mostly landward.

The cross-shore model CSHORE was calibrated for a rock structure placed directly on an eroding sand barrier with no filter. The mean and standard deviation of the free surface elevation and cross-shore velocity were predicted within errors of about 20% expect for small transmitted waves. The bed load parameter was increased by a factor of five to reproduce the degree of the profile deformation of the sand barrier without and with the rock mound and cover. The model CSHORE allows stone settlement but neglects stone spreading and sand exposure. The stone spreading and sand exposure will need to be examine in detail and incorporated into the model CSHORE.

Chapter 1

INTRODUCTION

Low-laying barrier islands and beaches, which are common along the U.S. East Coast, are vulnerable to wave overwash and breaching by storm surge and waves. Barrier island morphological changes induced by storms were observed in a number of studies (e.g., Claudino-Sales et al. 2010, Coogan et al. 2019) and simulated numerically by various researchers (e.g., Smallegan and Irish 2017, Harter and Figlus 2017). This study explores the possible use of a rubble mound structure in reducing the landward migration and crest lowering of a sand barrier during a storm. Hurricane Katrina cut a 2-km wide channel through a segment of the undeveloped section of Dauphin Island, Alabama in 2005 (Froede 2008). A rubble mound structure was constructed across the channel to close the Katrina cut (Webb et al. 2011) and a beach was formed on the seaward side of the structure during 2011 – 2019 (Gonzalez et al. 2020). On the other hand, a buried rock seawall reduced damage to the area landward of the seawall at Bay Head, New Jersey during Hurricane Sandy in 2012 (Irish et al. 2013). Kobayashi and Kim (2017) conducted a laboratory experiment to examine the effectiveness of a rock (stone) seawall in reducing wave overtopping and overwash of a sand beach. Their experiment is extended in this study to a sand barrier and wave transmission to a bay.

Claudino-Sales et al. (2010) examined dune erosion on Santa Rosa Island, Florida by Hurricane Ivan in 2004. The cross-island profiles before and after the storm indicated increased erosion at locations where the paved road was destroyed. The intact road acted like a thin protective cover for sediment underneath the pavement. At present, the paved road is ignored for the conservative estimation of wave overtopping and overwash of a barrier beach between an ocean and a bay (e.g., Kobayashi and Zhu 2017). The accurate prediction of wave overtopping is important for an enclosed bay with accumulation of overtopped water and little water outflux (Strazzella et al. 2019). In this study, a single-layer stone cover on a sand barrier was used to mimic a fractured paved road crudely.

A laboratory experiment consisting of three tests was conducted in a wave flume to quantify the effects of a rock mound and a rock cover on the migration and crest lowering of a sand barrier caused by irregular wave transformation, breaking, overtopping, and transmission. In the following, the experimental setup and procedure for the three tests are described in detail in Chapter 2. Each test consisted of 30 runs with a total duration of 12,000 s. The rock mound and cover were placed on the sand barrier crest without any filter. The effect of no filter on the rock structure settlement may be significant in the zone of large erosion (Yuksel and Kobayashi 2020).

In Chapter 3, the hydrodynamic and morphological data for the three tests are analyzed and compared to assess the efficacies of the rock mound and cover in reducing the sand barrier deformation.

In Chapter 4, the cross-shore numerical model CSHORE (Kobayashi 2016) is presented concisely. The model CSHORE is compared with the three tests and its option of no filter is calibrated. The comparison of the measured and computed results is provided in Chapter 5 to evaluate the accuracy and limitation of the numerical model.

Finally, the findings of this study are summarized in Chapter 6.

Chapter 2

EXPERIMENT

The laboratory experiment was performed to investigate migration and crest lowering of a sand barrier in the University of Delaware "Sand Tank" located in the basement of the Dupont Hall. This chapter provides an overview of the experimental setup for three sand barrier tests. The detailed explanation of the experimental setup refers to Figlus et al. (2011).

2.1 Experimental Setup

2.1.1 Wave tank and profile building

The experiment was conducted in a wave tank of 30-m length, 2.5-m width, and 1.5-m height. A dividing wall along the middle of the wave tank was installed to reduce the amount of sand. Three test series were carried out in a 23 m long and 1.15 m wide wave flume section of the entire wave tank. Figure 2.1 shows the schematic top view of the wave tank and the side view of the wave flume. A 400-s run of irregular waves corresponding to a Texel, Marsen, and Arsloe (TMA) spectrum was generated by a piston-type wave maker equipped at one end of the wave tank. The spectral significant wave height and peak period were approximately 20 cm and 2.6 s, respectively. Wave-absorbing slopes constructed of large rocks were located at the other end of the wave tank and at the end of the flume in front of the collection basin (not used in this experiment) to reduce wave reflection and seiche generation.

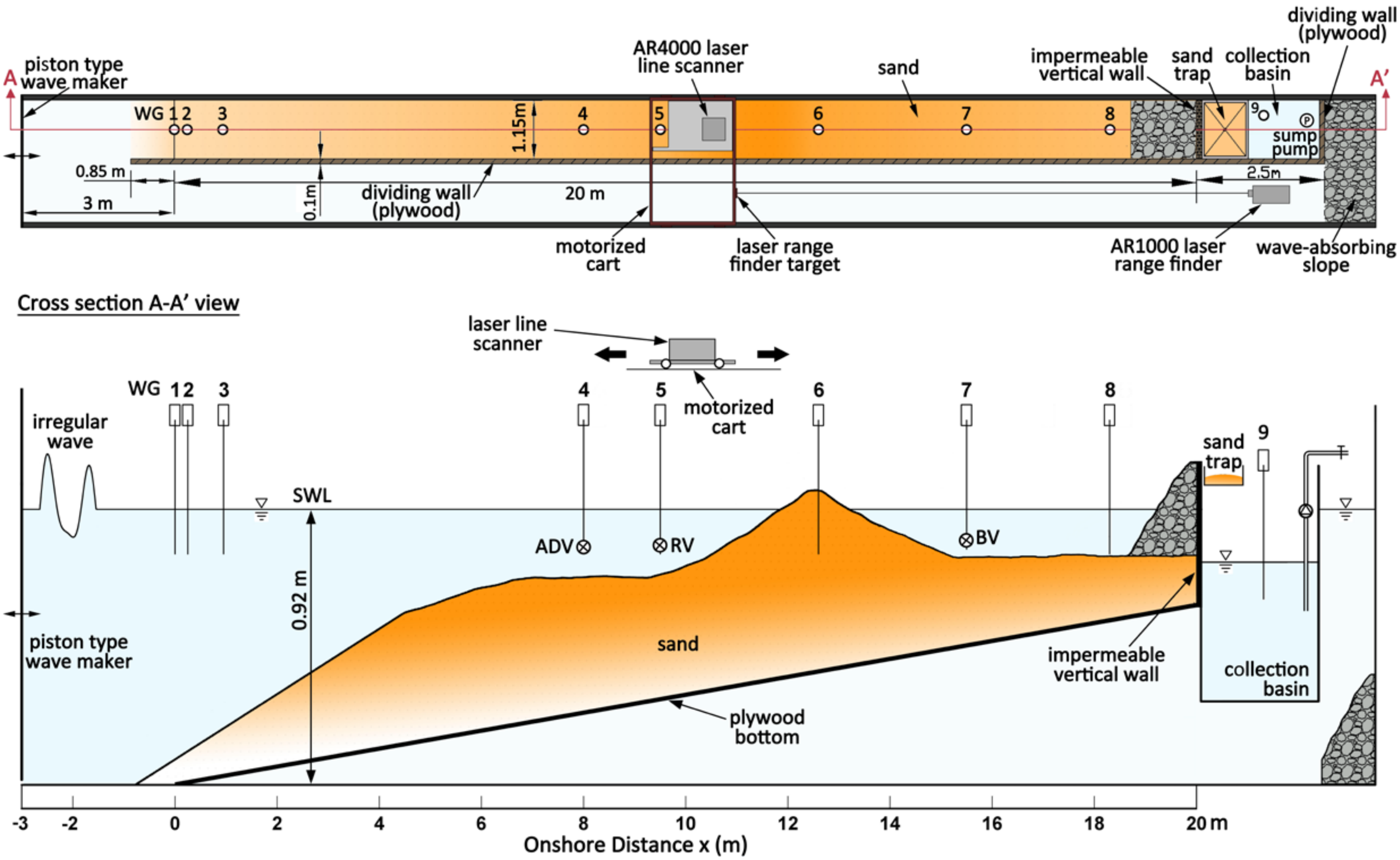

Figure 2.1 Experimental setup in 1.15 m wide flume at start of Test N with no structure

A rigid plywood was installed at a slope of 1/30 (vertical/horizontal) in the wave flume to reduce sand volume required in the flume. The sand beach on the plywood consisted of well-sorted fine sand with a median diameter of 0.18 mm. The fall velocity, specific gravity, and porosity of sand are 2.0 cm/s, 2.6 g/cm^3, and 0.4, respectively. The black fabric mesh was placed on the dividing wall, plywood, and impermeable side wall of the wave flume to enclose the sand and reduce sand leakage. The initial beach profile in Figure 2.1 represents a sand barrier with no structure. The side slopes of the initial sand barrier were about 0.1. The sand barrier does not represent a specific barrier island or beach because of the relatively narrow width. Fine sand used in this small-scale experiment might be considered as coarse sand on a prototype scale.

2.1.2 Measurement instruments and coordinate system

Eight capacitance wave gauges (WG1-WG8) were installed across the sand barrier to measure the free surface elevations above the still water level (SWL). The locations of each wave gauge are tabulated in Table 2.1. The cross-shore coordinate x is positive onshore starting from $x = 0$ at WG1 and ending at $x = 18.6$ m in front of the rock slope in the wave flume. The alongshore coordinate y is positive to the left from the direction of wave propagation with $y = 0$ along the center line of the wave flume. The vertical coordinate z is positive upward with $z = 0$ at SWL. WG1, WG2, and WG3 were located offshore to separate incident and reflected wave signals and examine the repeatability of each 400-s run. WG4 and WG5 were in the surf zone, and WG6 was initially situated on the emerged crest of the sand barrier. WG7 and WG8 were in the bay (transmission zone) landward of the sand barrier.

Three acoustic velocimeters consisting of one 2D ADV (Acoustic Doppler Velocimeter) and two 3D Vectrinos (Nortek, Rud, Norway) were used to record fluid velocities. ADV and Red Vectrino (RV) were co-located with WG4 and WG5 at an alongshore distance of 0.15 m from the flume center line. Blue Vectrino (BV) was located 0.1-m seaward of WG7 along the center line of the wave flume. In order to measure representative fluid velocities, the velocimeters were placed at an elevation of one-third of the local depth above the sediment bottom and adjusted vertically after each run.

Table 2.1 Wave gauge locations (WG1-WG8) and velocimeter locations (ADV; Red-Vectrino, RV; and Blue-Vectrino, BV)

Wave Gauge	**WG1**	**WG2**	**WG3**	**WG4**	**WG5**	**WG6**	**WG7**	**WG8**
***x* (m)**	0.00	0.25	0.95	8.00	9.50	12.60	15.50	18.30
***y* (m)**	0.00	0.00	0.00	0.00	0.00	0.00	0.00	0.00
Velocity Gauge				**ADV**	**RV**		**BV**	
***x* (m)**				8.00	9.50		15.40	
***y* (m)**				0.15	0.15		0.00	
***z* (m)**				$-2d/3$	$-2d/3$		$-2d/3$	

d = local water depth at the start of each run
x = onshore coordinate with $x = 0$ at WG1
y = alongshore coordinate with $y = 0$ at the middle of the wave flume
z = vertical coordinate with $z = 0$ at SWL

Beach profiles seaward of the wave-absorbing slope in Figure 2.1 were measured by the combination of a class III Acuity AR4000-LIR laser line scanner mounted on a motorized cart and a fixed class II Acuity AR1000 laser range finder situated next to the collection basin. The laser scanner system can obtain 3D bathymetry of the subaerial bed surface after draining water in the wave tank. The error of the measured profile elevation was 1 mm. The collection basin, together with a sand trap, collected the transported water and sand over the impermeable vertical wall to calculate the averaged wave overtopping rate and sand overwash rate during each 400-s run. No wave overtopping and sand overwash over the wall occurred in this experiment.

2.2 Experimental procedure

Three tests were conducted in the wave flume with the water depth of 92 cm to compare the landward migration and crest lowering of the sand barrier with and without structure protection: no structure (N), rock mound (R), and rock cover (C). The initial profiles averaged in the alongshore direction as well as the corresponding experiment photos are shown in Figure 2.2.

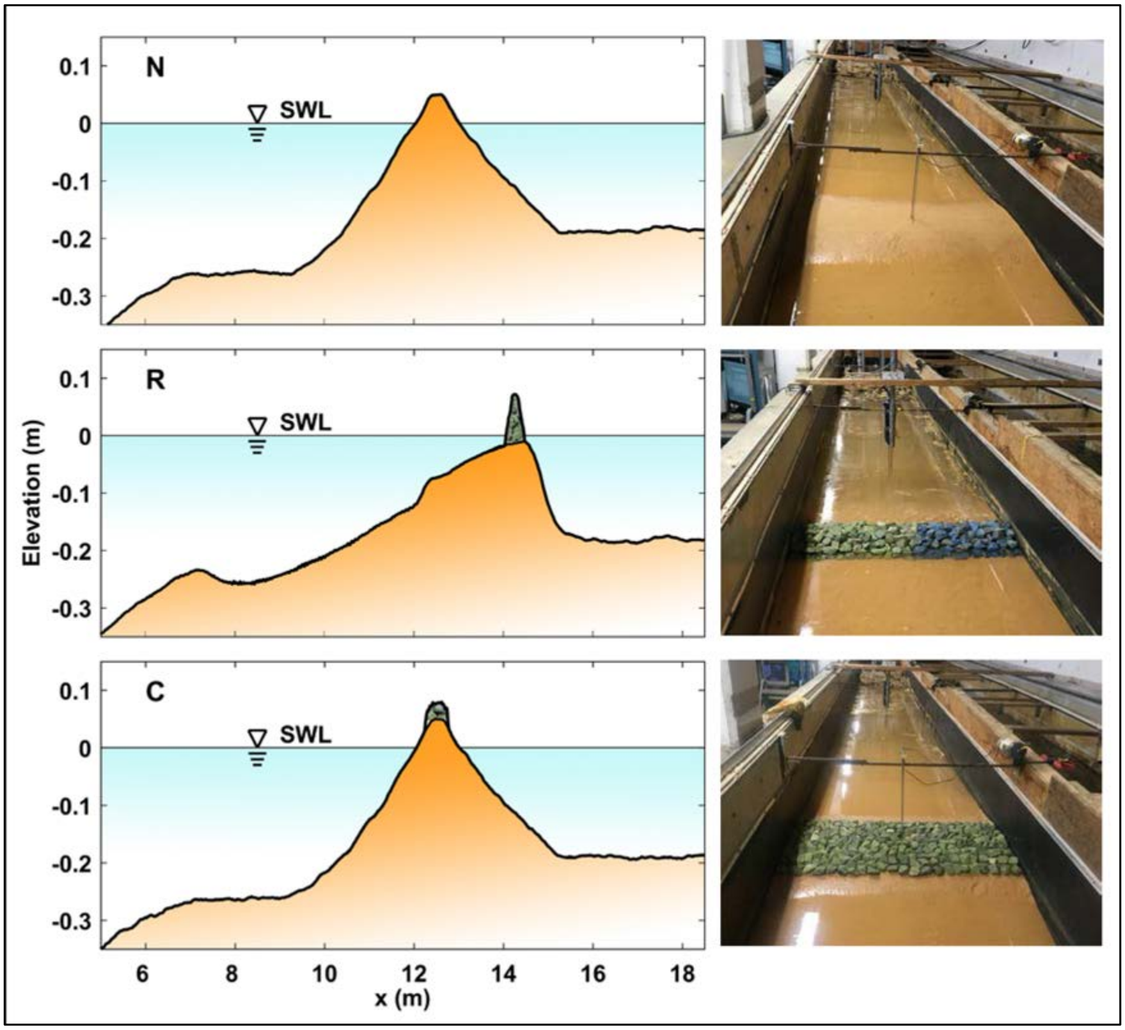

Figure 2.2 Initial profiles and photos of Tests N, R, and C with Still Water Level (SWL) of 92 cm in the wave flume

Table 2.2 Sequence of three tests to reduce sand barrier migration and crest lowering by a rock mound or cover

Test	Structure	No. of Runs	Description
N	No Structure	30	onshore migration and crest lowing of a sand barrier (idealized barrier island)
R	Rock Mound	30	rock mound on the lowered sand barrier
C	Rock Cover	30	rock cover (fractured paved road) on the initial crest of the sand barrier

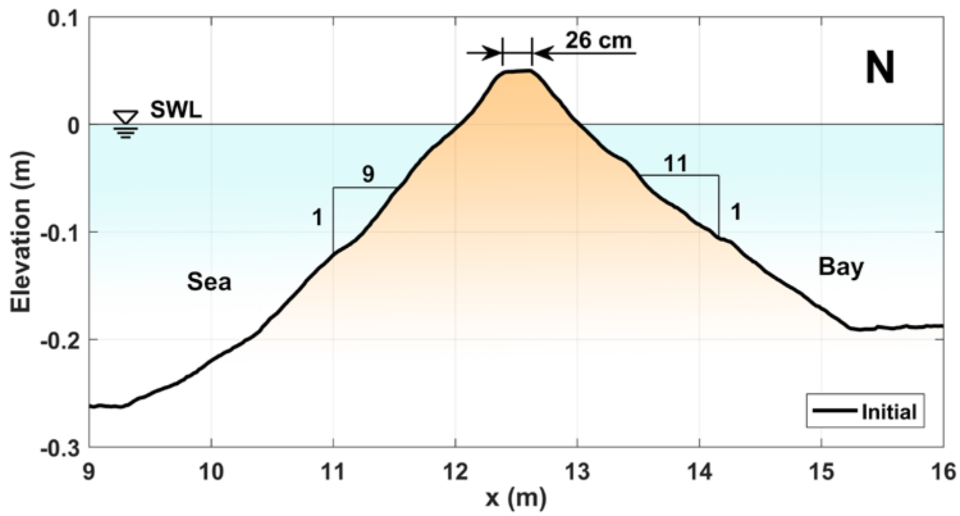

Figure 2.3 Initial profile with no structure for Test N

Table 2.2 outlines three tests in sequence. For Test N with no structure, a sand barrier was built artificially in the range of x = 9.3 – 15.3 m to examine the morphodynamics of a narrow barrier (26-cm crest width) during a storm (Figure 2.3). The crest of the barrier was emerged initially where the seaward and landward slopes were approximately 1/9 and 1/11, respectively. Pronounced crest lowering was observed after 5 runs with each run lasting 400-s and the beach profile was measured after 5 runs. The sand mound was gradually migrating onshore and the profile was measured after 10, 20, and 30 runs where the run number is from the start of Test N. Test N was terminated after 30 runs when the barrier crest became submerged. The barrier profile with alongshore inclination was adjusted alongshore before the profile measurement. This profile adjustment did not change the alongshore averaged profile.

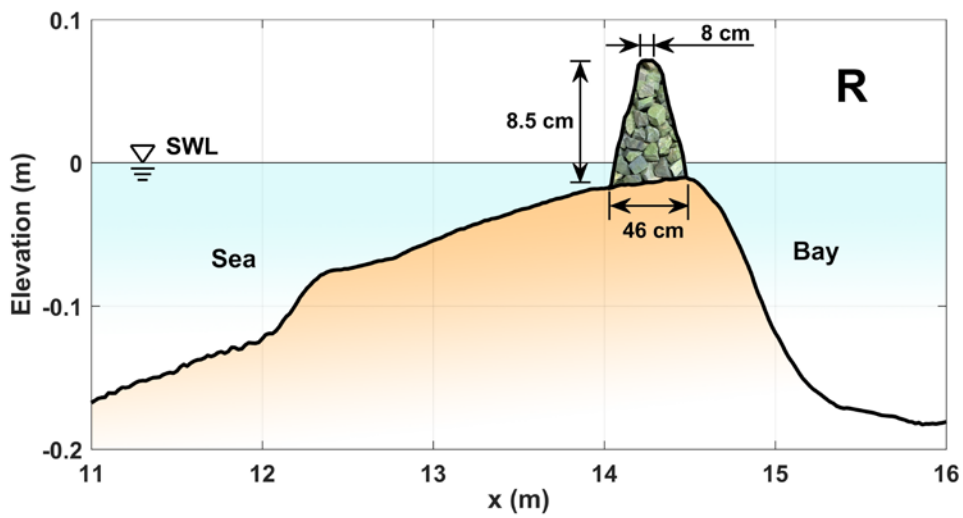

Figure 2.4 Initial profile of Test R with a rock mound built on the submerged sand barrier at the end of Test N

The final profile of Test N was submerged after 30 runs of irregular waves with a total duration of 12,000 s. In order to reduce the crest lowering and onshore movement of the sand barrier, a rock mound was placed directly on the top of the barrier without any filter because of the difficulty in placing fabric mesh under water in the field, as depicted in Figure 2.4. The rock mound was constructed of the green and blue stones used by Kobayashi and Kim (2017) with the crest elevation above SWL. The nominal diameter, specific gravity, and porosity were 3.52 cm, 2.94, and 0.44 for the green stones, and 3.81 cm, 3.06, and 0.44 for the blue stones.

The surface and bottom widths of the rock mound were 8 and 46 cm, respectively. The alongshore widths of the green and blue stones were 62 and 53 cm in the 115 cm wide flume. The stones were placed carefully by hand in a three-layer thickness with a height of 8.5 cm. The front and back slopes were about 1/2. The testing procedure for Test N was repeated with the same SWL and the profiles were measured after 5, 10, 20, and 30 runs. The rock mound located in the zone of x = 14.02 – 14.48 m settled downward. The stones did not move under wave action. At the end of Test R, the stones were removed carefully so as to measure the sand surface elevation including sand particles deposited inside the rock mound. After the stone removal, the sand surface was smoothed and measured after Test R.

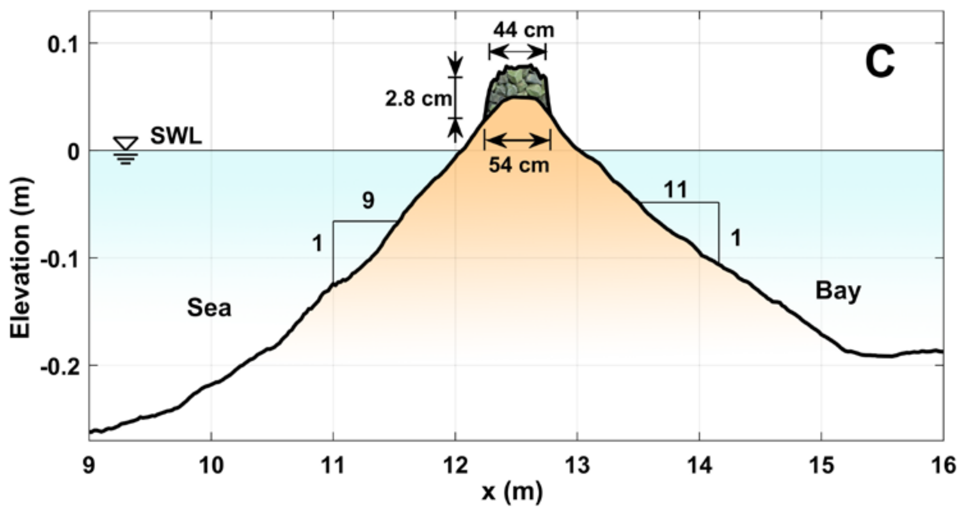

Figure 2.5 Initial profile of Test C with a rock cover built on the initial profile of Test N

The sand barrier was rebuilt for Test C. The initial sand barrier profile for Test C was almost the same (within 1 cm) as the initial profile of Test N. A single layer rock cover consisting of the green stones only was placed over the crest of the sand barrier in the zone of x = 12.24 – 12.78 m with no filter, as depicted in Figure 2.5. The rock cover might be regarded as a fractured paved road on a barrier island or beach to quantify the effect of the paved road on the sand barrier erosion during a storm. The surface and bottom widths of the rock cover were 44 and 54 cm, respectively. The alongshore length and average height of the rock cover were 115 cm and 2.8 cm, respectively. The average height was less than the nominal green stone diameter of 3.52 cm because of the irregular stone surface. The testing procedure for Test C was the same as that for Test R. The major difference between the two tests was the rock layer thickness. The green stones did not move under wave action but settled and dispersed because of erosion of sand particles in the vicinity of each stone.

Chapter 3

DATA ANALYSIS

The experimental data are analyzed and presented in this chapter. Measurements included hydrodynamics and barrier beach profile evolution. Sand volume changes as well as rock settlement and spreading are examined to evaluate the efficacy of the rock mound and cover in reducing the sand barrier deformation.

3.1 Hydrodynamics

The incident wave characteristics and reflection coefficient at the location of x = 0 of WG1 for Tests N, R, and C are listed in Tables 3.1 – 3.3, where H_{mo} = spectral significant wave height, H_{rms} = root-mean-square wave height, H_s = significant wave height, T_p = spectral wave period, T_s = significant wave period, and R = wave reflection coefficient. The spectral significant wave height H_{mo} and wave period T_p were approximately 20 cm and 2.6 s. The average reflection coefficient was 0.13, 0.15, and 0.14 for Tests N, R, and C, respectively. The effect of the rock mound and cover on the wave reflection was small because of the dissipation of incident wave energy on the front beach.

Tables 3.4 – 3.9 list the mean $\bar{\eta}$ and standard deviation σ_η of the free surface elevation η above SWL at the eight wave gauges for each run of Tests N, R, and C. The mean $\bar{u}$ and standard deviation σ_u of the cross-shore velocity u measured by ADV, RV, and BV are tabulated in Tables 3.10 – 3.12. The measured alongshore and vertical velocities were small in comparison with the cross-shore velocities. The values of $\bar{\eta}$, σ_η, $\bar{u}$, and σ_u are analyzed to examine the cross-shore wave transformation.

Table 3.1 Incident wave characteristics, Test N.

Run	H_{mo} **(cm)**	H_{rms} **(cm)**	H_s **(cm)**	T_p **(s)**	T_s **(s)**	R
N1	19.31	13.65	18.72	2.62	2.14	0.150
N2	19.94	14.10	19.35	2.62	2.13	0.137
N3	18.81	13.30	18.33	2.62	2.12	0.133
N4	20.15	14.25	19.47	2.62	2.12	0.137
N5	20.11	14.22	19.54	2.62	2.16	0.130
N6	19.08	13.49	18.42	2.62	2.16	0.133
N7	19.81	14.01	19.20	2.62	2.13	0.136
N8	19.99	14.14	19.40	2.62	2.14	0.137
N9	20.09	14.20	19.45	2.62	2.16	0.135
N10	20.06	14.18	19.43	2.62	2.13	0.132
N11	19.06	13.48	18.46	2.62	2.17	0.127
N12	19.84	14.03	19.23	2.62	2.14	0.133
N13	20.04	14.17	19.39	2.62	2.14	0.132
N14	20.18	14.27	19.48	2.62	2.15	0.130
N15	20.24	14.31	19.55	2.62	2.15	0.134
N16	20.26	14.33	19.48	2.62	2.14	0.130
N17	20.20	14.28	19.43	2.62	2.11	0.133
N18	19.92	14.08	19.33	2.62	2.13	0.130
N19	18.27	12.92	17.85	2.62	2.17	0.125
N20	19.67	13.91	18.91	2.62	2.15	0.131
N21	NR	NR	NR	NR	NR	NR
N22	19.41	13.72	18.57	2.62	2.13	0.129
N23	19.53	13.81	18.81	2.62	2.13	0.123
N24	19.69	13.92	18.95	2.62	2.13	0.128
N25	19.70	13.93	18.92	2.62	2.13	0.129
N26	19.73	13.95	19.04	2.62	2.15	0.129
N27	19.68	13.92	18.99	2.62	2.12	0.128
N28	19.74	13.96	18.99	2.62	2.12	0.131
N29	19.69	13.92	18.99	2.62	2.12	0.128
N30	NR	NR	NR	NR	NR	NR
Avg.	**19.72**	**13.95**	**19.06**	**2.62**	**2.14**	**0.132**

NR implies "not reliable" data

Table 3.2 Incident wave characteristics, Test R.

Run	H_{mo} (cm)	H_{rms} (cm)	H_s (cm)	T_p (s)	T_s (s)	R
R1	19.61	13.87	19.07	2.62	2.15	0.146
R2	19.79	14.00	19.18	2.62	2.12	0.146
R3	20.04	14.17	19.36	2.62	2.13	0.144
R4	20.32	14.37	19.77	2.62	2.14	0.146
R5	20.50	14.49	19.75	2.62	2.12	0.143
R6	20.24	14.31	19.57	2.62	2.13	0.143
R7	20.62	14.58	19.93	2.62	2.14	0.145
R8	20.78	14.69	20.03	2.62	2.12	0.145
R9	20.82	14.72	20.22	2.62	2.15	0.145
R10	20.85	14.74	20.12	2.62	2.11	0.152
R11	19.84	14.03	19.36	2.62	2.13	0.149
R12	20.22	14.30	19.59	2.62	2.12	0.153
R13	20.45	14.46	19.75	2.62	2.12	0.153
R14	20.46	14.47	19.73	2.62	2.14	0.152
R15	20.49	14.49	19.88	2.62	2.14	0.152
R16	20.45	14.46	19.74	2.62	2.13	0.155
R17	20.43	14.45	19.73	2.62	2.13	0.157
R18	20.39	14.42	19.71	2.62	2.13	0.157
R19	20.32	14.37	19.72	2.62	2.11	0.160
R20	20.24	14.31	19.60	2.62	2.12	0.160
R21	19.96	14.11	19.35	2.62	2.14	0.162
R22	20.25	14.32	19.57	2.62	2.14	0.157
R23	20.18	14.27	19.49	2.62	2.12	0.159
R24	20.31	14.36	19.62	2.62	2.12	0.159
R25	20.31	14.36	19.53	2.62	2.11	0.165
R26	20.24	14.31	19.58	2.62	2.12	0.163
R27	20.25	14.32	19.52	2.62	2.15	0.160
R28	20.17	14.26	19.48	2.62	2.14	0.159
R29	20.08	14.20	19.46	2.62	2.11	0.163
R30	20.05	14.18	19.35	2.62	2.14	0.159
Avg.	**20.29**	**14.35**	**19.63**	**2.62**	**2.13**	**0.154**

Table 3.3 Incident wave characteristics, Test C.

Run	H_{mo} (cm)	H_{rms} (cm)	H_s (cm)	T_p (s)	T_s (s)	R
C1	19.61	13.86	18.95	2.62	2.14	0.172
C2	20.12	14.23	19.40	2.62	2.15	0.151
C3	20.06	14.18	19.42	2.62	2.14	0.143
C4	19.97	14.12	19.32	2.62	2.17	0.142
C5	19.95	14.10	19.38	2.62	2.15	0.146
C6	18.81	13.30	18.20	2.62	2.17	0.136
C7	19.46	13.76	18.78	2.62	2.15	0.139
C8	19.41	13.72	18.89	2.62	2.17	0.142
C9	19.36	13.69	18.68	2.62	2.15	0.136
C10	19.37	13.69	18.87	2.62	2.15	0.141
C11	18.52	13.10	17.97	2.62	2.18	0.134
C12	18.97	13.41	18.37	2.62	2.17	0.134
C13	19.11	13.51	18.50	2.62	2.17	0.146
C14	18.92	13.37	18.33	2.62	2.18	0.136
C15	18.94	13.39	18.42	2.62	2.15	0.144
C16	18.90	13.37	18.26	2.62	2.14	0.141
C17	18.82	13.31	18.10	2.62	2.14	0.138
C18	18.77	13.27	18.19	2.62	2.17	0.138
C19	18.69	13.22	18.13	2.62	2.13	0.140
C20	18.64	13.18	18.10	2.62	2.15	0.137
C21	17.46	12.34	16.87	2.62	2.16	0.133
C22	17.76	12.56	17.17	2.62	2.17	0.134
C23	18.02	12.74	17.40	2.62	2.12	0.134
C24	18.13	12.82	17.42	2.62	2.14	0.134
C25	18.08	12.78	17.52	2.62	2.15	0.128
C26	18.05	12.76	17.36	2.62	2.14	0.132
C27	18.04	12.75	17.38	2.62	2.13	0.136
C28	17.98	12.72	17.50	2.62	2.17	0.131
C29	17.90	12.66	17.42	2.62	2.15	0.137
C30	17.82	12.60	17.20	2.62	2.15	0.132
Avg.	**18.79**	**13.28**	**18.18**	**2.62**	**2.15**	**0.139**

Table 3.4 Mean free-surface elevation $\overline{\eta}$ (cm) at 8 wave gauge locations, Test N.

Run	WG1	WG2	WG3	WG4	WG5	WG6	WG7	WG8
N1	-0.62	-0.55	-0.69	-0.41	-0.34	NR	4.75	4.38
N2	-0.51	-0.57	-0.56	-0.32	-0.22	1.74	3.36	3.26
N3	-0.36	-0.43	-0.48	-0.26	-0.28	1.42	2.69	2.68
N4	-0.40	-0.42	-0.52	-0.24	-0.16	1.44	2.85	2.79
N5	-0.43	-0.46	-0.52	-0.26	-0.19	1.33	3.10	2.94
N6	-0.46	-0.56	-0.50	-0.29	-0.20	1.12	2.83	2.84
N7	-0.47	-0.48	-0.51	-0.25	-0.20	1.14	2.91	2.86
N8	-0.42	-0.48	-0.50	-0.23	-0.32	1.11	2.88	2.81
N9	-0.39	-0.48	-0.49	-0.20	-0.15	1.06	2.88	2.84
N10	-0.38	-0.46	-0.51	-0.22	-0.14	0.99	2.84	2.80
N11	-0.44	-0.47	-0.54	-0.25	-0.18	0.84	2.86	2.88
N12	-0.43	-0.46	-0.51	-0.05	-0.17	0.87	2.91	2.87
N13	-0.41	-0.45	-0.53	-0.22	-0.15	0.87	2.89	2.88
N14	-0.40	-0.47	-0.53	-0.24	-0.16	0.83	2.87	2.94
N15	-0.41	-0.45	-0.46	-0.22	-0.04	0.77	2.84	2.82
N16	-0.40	-0.48	-0.52	-0.20	-0.12	0.75	2.83	2.87
N17	-0.42	-0.48	-0.49	-0.18	-0.12	0.64	2.80	2.79
N18	-0.38	-0.44	-0.46	-0.16	-0.12	0.59	2.72	2.78
N19	-0.33	-0.38	-0.42	-0.23	-0.19	0.46	2.58	2.61
N20	-0.37	-0.45	-0.47	-0.20	-0.12	0.52	2.62	2.69
N21	NR	NR	NR	NR	NR	NR	NR	NR
N22	-0.36	-0.42	-0.49	-0.19	-0.14	0.50	2.45	2.47
N23	-0.35	-0.41	-0.50	-0.17	-0.14	0.48	2.48	2.49
N24	-0.34	-0.39	-0.47	-0.19	-0.12	0.48	2.41	2.40
N25	-0.37	-0.38	-0.47	-0.18	-0.10	0.35	2.39	2.42
N26	-0.33	-0.40	-0.45	-0.16	-0.08	0.42	2.35	2.34
N27	-0.32	-0.38	-0.44	-0.16	-0.08	0.38	2.31	2.29
N28	-0.33	-0.38	-0.46	-0.15	-0.07	0.33	2.29	2.31
N29	-0.30	-0.36	-0.42	-0.11	-0.07	0.33	2.20	2.21
N30	NR	NR	NR	NR	NR	NR	NR	NR
Avg.	**-0.40**	**-0.45**	**-0.50**	**-0.21**	**-0.16**	**0.81**	**2.78**	**2.76**

NR implies "not reliable" data

Table 3.5 Mean free-surface elevation $\overline{\eta}$ (cm) at 8 wave gauge locations, Test R.

Run	WG1	WG2	WG3	WG4	WG5	WG6	WG7	WG8
R1	-0.34	-0.38	-0.46	-0.17	-0.11	0.18	3.13	2.87
R2	-0.40	-0.42	-0.48	-0.16	-0.11	0.14	3.21	3.10
R3	-0.36	-0.41	-0.50	-0.18	-0.11	0.14	3.26	3.19
R4	-0.41	-0.47	-0.51	-0.16	-0.08	0.15	3.37	3.30
R5	-0.42	-0.49	-0.50	-0.19	-0.11	0.11	3.44	3.37
R6	-0.43	-0.44	-0.44	-0.15	-0.12	-0.01	3.71	3.53
R7	-0.41	-0.47	-0.48	-0.16	-0.10	0.11	3.62	3.54
R8	-0.40	-0.47	-0.48	-0.16	-0.07	0.14	3.68	3.65
R9	-0.42	-0.46	-0.45	-0.16	-0.08	0.19	3.77	3.71
R10	-0.43	-0.48	-0.55	-0.17	-0.06	0.17	3.82	3.80
R11	-0.44	-0.47	-0.53	-0.16	-0.10	0.07	3.85	3.76
R12	-0.40	-0.46	-0.46	-0.17	-0.10	0.13	3.88	3.61
R13	-0.42	-0.48	-0.47	-0.14	-0.11	0.17	3.93	3.76
R14	-0.43	-0.50	-0.49	-0.15	-0.08	0.14	3.91	3.85
R15	-0.39	-0.45	-0.46	-0.11	-0.07	0.14	3.77	3.53
R16	-0.40	-0.47	-0.47	-0.11	-0.07	0.15	3.88	3.61
R17	-0.40	-0.49	-0.48	-0.11	-0.08	0.14	3.66	3.80
R18	-0.38	-0.44	-0.44	-0.12	-0.04	0.18	3.65	3.59
R19	-0.44	-0.49	-0.47	-0.10	-0.06	0.15	3.83	3.76
R20	-0.40	-0.48	-0.44	-0.13	-0.05	0.15	3.76	3.72
R21	-0.38	-0.42	-0.49	-0.11	-0.02	0.18	3.77	3.65
R22	-0.37	-0.45	-0.53	-0.10	-0.03	0.16	3.70	3.67
R23	-0.45	-0.47	-0.55	-0.11	-0.07	0.16	3.81	3.79
R24	-0.39	-0.48	-0.51	-0.11	-0.05	0.16	3.80	3.58
R25	-0.37	-0.44	-0.51	-0.12	-0.03	0.17	3.78	3.68
R26	-0.40	-0.49	-0.51	-0.11	-0.05	0.14	3.62	3.75
R27	-0.38	-0.48	-0.51	-0.11	-0.04	0.09	3.75	3.68
R28	-0.40	-0.49	-0.49	-0.11	-0.05	0.12	3.81	3.76
R29	-0.40	-0.46	-0.50	-0.10	-0.07	0.12	3.84	3.82
R30	-0.41	-0.42	-0.52	-0.12	-0.05	0.12	3.87	3.82
Avg.	**-0.40**	**-0.46**	**-0.49**	**-0.14**	**-0.07**	**0.14**	**3.70**	**3.61**

Table 3.6 Mean free-surface elevation $\overline{\eta}$ (cm) at 8 wave gauge locations, Test C.

Run	WG1	WG2	WG3	WG4	WG5	WG6	WG7	WG8
C1	-0.62	-0.68	-0.76	-0.51	-0.42	0.14	5.51	5.09
C2	-0.55	-0.58	-0.71	-0.38	-0.32	2.70	3.78	3.75
C3	-0.55	-0.57	-0.62	-0.36	-0.29	2.29	3.51	2.39
C4	-0.47	-0.64	-0.56	-0.30	-0.25	2.14	3.43	3.47
C5	-0.45	-0.54	-0.56	-0.30	-0.25	2.03	3.20	3.32
C6	-0.45	-0.50	-0.62	-0.34	-0.31	1.81	3.44	3.30
C7	-0.52	-0.51	-0.61	-0.30	-0.32	1.78	3.38	3.31
C8	-0.44	-0.48	-0.57	-0.28	-0.24	1.75	3.32	3.27
C9	-0.46	-0.53	-0.60	-0.29	-0.23	1.74	3.27	3.22
C10	-0.38	-0.49	-0.53	-0.28	-0.23	1.67	3.16	3.25
C11	-0.39	-0.44	-0.56	-0.32	-0.29	1.30	3.08	3.01
C12	-0.41	-0.49	-0.55	-0.27	-0.25	1.41	3.11	3.10
C13	-0.41	-0.46	-0.53	-0.29	-0.24	1.20	3.12	3.06
C14	-0.43	-0.49	-0.54	-0.30	-0.26	1.42	3.12	3.07
C15	-0.43	-0.49	-0.52	-0.28	-0.25	1.22	3.11	3.10
C16	-0.40	-0.49	-0.53	-0.29	-0.25	1.27	3.08	3.06
C17	-0.40	-0.48	-0.53	-0.30	-0.24	1.41	3.05	2.93
C18	-0.40	-0.46	-0.52	-0.30	-0.24	1.65	3.06	3.05
C19	-0.39	-0.45	-0.53	-0.30	-0.25	0.58	3.05	3.01
C20	-0.41	-0.48	-0.52	-0.29	-0.25	1.09	3.05	3.00
C21	-0.37	-0.40	-0.51	-0.30	-0.26	1.00	2.87	2.81
C22	-0.43	-0.47	-0.55	-0.29	-0.30	0.95	2.85	2.82
C23	-0.37	-0.47	-0.46	-0.29	-0.27	0.92	2.87	2.77
C24	-0.35	-0.42	-0.53	-0.29	-0.25	0.91	2.86	2.87
C25	-0.38	-0.43	-0.47	-0.28	-0.25	0.85	2.84	2.84
C26	-0.34	-0.42	-0.46	-0.27	-0.23	0.86	2.84	2.90
C27	-0.34	-0.41	-0.45	-0.26	-0.19	0.92	2.85	2.86
C28	-0.35	-0.40	-0.45	-0.26	-0.23	0.77	2.82	2.79
C29	-0.38	-0.43	-0.45	-0.26	-0.20	0.80	2.79	2.78
C30	-0.37	-0.42	-0.44	-0.25	-0.22	0.87	2.79	2.80
Avg.	**-0.42**	**-0.48**	**-0.54**	**-0.30**	**-0.26**	**1.32**	**3.17**	**3.10**

Table 3.7 Free-surface standard deviation σ_η (cm) at 8 wave gauge locations, Test N.

Run	**WG1**	**WG2**	**WG3**	**WG4**	**WG5**	**WG6**	**WG7**	**WG8**
N1	4.77	4.74	4.75	3.94	3.39	NR	0.82	0.75
N2	4.89	4.88	4.87	3.92	3.43	1.82	0.85	0.79
N3	4.61	4.61	4.62	3.80	3.33	1.90	0.83	0.82
N4	4.96	4.92	4.92	3.95	3.40	1.97	0.90	0.87
N5	4.94	4.93	4.92	3.91	3.41	1.98	0.93	0.90
N6	4.69	4.64	4.67	3.86	3.40	2.01	0.90	0.89
N7	4.88	4.83	4.84	3.93	3.45	2.06	0.92	0.91
N8	4.92	4.88	4.89	3.93	3.45	2.10	0.94	0.92
N9	4.96	4.89	4.90	3.93	3.47	2.12	0.94	0.92
N10	4.95	4.90	4.90	3.89	3.44	2.18	0.96	0.92
N11	4.69	4.62	4.67	3.86	3.41	2.11	0.86	0.84
N12	4.88	4.81	4.85	3.91	3.44	2.17	0.87	0.86
N13	4.93	4.87	4.90	3.90	3.43	2.17	0.87	0.86
N14	4.98	4.91	4.93	3.91	3.43	2.24	0.88	0.86
N15	4.99	4.93	4.94	3.90	3.41	2.25	0.89	0.87
N16	4.99	4.94	4.95	3.90	3.42	2.27	0.91	0.88
N17	4.99	4.92	4.92	3.89	3.40	2.31	0.90	0.87
N18	4.91	4.86	4.86	3.88	3.43	2.35	0.90	0.86
N19	4.52	4.47	4.46	3.69	3.31	2.32	0.90	0.86
N20	4.85	4.80	4.79	3.84	3.37	2.39	0.90	0.85
N21	NR	NR	NR	NR	NR	NR	NR	NR
N22	4.76	4.75	4.75	3.80	3.38	2.40	0.93	0.85
N23	4.80	4.79	4.78	3.80	3.39	2.41	0.93	0.86
N24	4.83	4.83	4.80	3.77	3.39	2.44	0.94	0.87
N25	4.83	4.83	4.81	3.84	3.38	2.44	0.95	0.87
N26	4.84	4.84	4.81	3.80	3.42	2.50	0.96	0.88
N27	4.83	4.82	4.80	3.79	3.41	2.49	0.96	0.88
N28	4.84	4.84	4.81	3.80	3.40	2.49	0.98	0.89
N29	4.84	4.83	4.81	3.80	3.39	2.52	0.99	0.90
N30	NR	NR	NR	NR	NR	NR	NR	NR
Avg.	**4.85**	**4.82**	**4.82**	**3.86**	**3.41**	**2.24**	**0.91**	**0.87**

NR implies "not reliable" data

Table 3.8 Free-surface standard deviation σ_η (cm) at 8 wave gauge locations, Test R.

Run	WG1	WG2	WG3	WG4	WG5	WG6	WG7	WG8
R1	4.83	4.81	4.79	3.80	3.36	2.55	0.59	0.52
R2	4.88	4.85	4.82	3.81	3.38	2.59	0.62	0.52
R3	4.95	4.92	4.87	3.81	3.38	2.61	0.61	0.56
R4	5.02	4.98	4.93	3.82	3.41	2.67	0.64	0.56
R5	5.06	5.03	4.98	3.85	3.44	2.77	0.66	0.59
R6	4.99	4.92	4.95	3.84	3.44	2.79	0.66	0.58
R7	5.10	5.02	5.03	3.86	3.41	2.80	0.67	0.59
R8	5.14	5.07	5.05	3.85	3.42	2.81	0.69	0.59
R9	5.15	5.09	5.07	3.86	3.46	2.80	0.68	0.60
R10	5.15	5.09	5.07	3.85	3.41	2.83	0.68	0.60
R11	4.88	4.82	4.87	3.78	3.34	2.77	0.67	0.59
R12	4.98	4.92	4.94	3.81	3.37	2.83	0.67	0.57
R13	5.04	4.98	5.00	3.83	3.37	2.84	0.68	0.56
R14	5.04	4.98	5.01	3.82	3.38	2.86	0.69	0.59
R15	5.05	4.99	5.03	3.81	3.37	2.85	0.68	0.57
R16	5.05	4.98	5.01	3.80	3.36	2.86	0.68	0.59
R17	5.04	4.99	5.00	3.80	3.35	2.87	0.67	0.57
R18	5.03	4.98	4.98	3.79	3.40	2.87	0.67	0.56
R19	5.02	4.96	4.96	3.77	3.36	2.86	0.66	0.57
R20	5.00	4.95	4.95	3.76	3.36	2.88	0.66	0.57
R21	4.91	4.85	4.89	3.72	3.32	2.82	0.63	0.55
R22	5.00	4.93	4.97	3.77	3.32	2.84	0.64	0.56
R23	4.98	4.92	4.95	3.77	3.33	2.86	0.66	0.56
R24	5.01	4.96	4.97	3.77	3.34	2.87	0.67	0.57
R25	5.00	4.95	4.96	3.76	3.32	2.90	0.68	0.57
R26	4.99	4.95	4.95	3.77	3.30	2.90	0.68	0.57
R27	4.99	4.95	4.95	3.77	3.30	2.89	0.69	0.58
R28	4.97	4.94	4.94	3.78	3.31	2.91	0.71	0.60
R29	4.94	4.91	4.91	3.75	3.30	2.91	0.70	0.60
R30	4.94	4.91	4.91	3.74	3.29	2.91	0.71	0.59
Avg.	**5.00**	**4.95**	**4.96**	**3.80**	**3.36**	**2.82**	**0.67**	**0.57**

Table 3.9 Free-surface standard deviation σ_η (cm) at 8 wave gauge locations, Test C.

Run	**WG1**	**WG2**	**WG3**	**WG4**	**WG5**	**WG6**	**WG7**	**WG8**
C1	4.88	4.83	4.79	3.99	3.54	1.48	1.08	0.94
C2	4.98	4.91	4.89	3.97	3.51	1.70	0.86	0.78
C3	4.94	4.90	4.87	3.91	3.50	1.84	0.90	0.84
C4	4.93	4.87	4.85	3.94	3.50	1.85	0.94	0.87
C5	4.91	4.86	4.84	3.91	3.46	1.85	0.94	0.88
C6	4.62	4.58	4.60	3.76	3.36	1.87	0.90	0.87
C7	4.77	4.75	4.75	3.84	3.42	1.90	0.93	0.90
C8	4.75	4.75	4.73	3.81	3.42	1.90	0.93	0.91
C9	4.74	4.73	4.73	3.82	3.44	1.92	0.94	0.90
C10	4.77	4.74	4.72	3.82	3.42	1.95	0.94	0.89
C11	4.52	4.50	4.55	3.77	3.41	1.84	0.89	0.86
C12	4.64	4.61	4.65	3.82	3.44	1.98	0.90	0.87
C13	4.67	4.64	4.67	3.80	3.43	1.98	0.90	0.87
C14	4.62	4.61	4.63	3.80	3.43	2.05	0.90	0.87
C15	4.63	4.61	4.62	3.82	3.42	2.11	0.90	0.86
C16	4.63	4.61	4.62	3.79	3.45	2.12	0.91	0.88
C17	4.61	4.59	4.59	3.75	3.42	2.10	0.90	0.88
C18	4.60	4.59	4.59	3.78	3.41	2.11	0.91	0.88
C19	4.58	4.57	4.56	3.76	3.39	2.14	0.91	0.88
C20	4.57	4.56	4.55	3.76	3.42	2.19	0.92	0.87
C21	4.27	4.25	4.29	3.66	3.35	2.21	0.88	0.84
C22	4.35	4.35	4.33	3.69	3.34	2.15	0.90	0.85
C23	4.41	4.42	4.39	3.70	3.36	2.19	0.89	0.86
C24	4.44	4.45	4.42	3.69	3.37	2.19	0.92	0.86
C25	4.43	4.44	4.41	3.72	3.36	2.20	0.91	0.86
C26	4.41	4.43	4.40	3.71	3.34	2.23	0.91	0.87
C27	4.41	4.43	4.39	3.69	3.35	2.23	0.92	0.87
C28	4.40	4.42	4.38	3.69	3.32	2.20	0.94	0.88
C29	4.38	4.40	4.36	3.69	3.32	2.20	0.93	0.86
C30	4.36	4.38	4.34	3.66	3.33	2.52	0.94	0.87
Avg.	**4.61**	**4.59**	**4.58**	**3.78**	**3.41**	**2.04**	**0.92**	**0.87**

Table 3.10 Mean $\overline{u}$ and standard deviation σ_u of measured cross-shore velocity u, Test N.

Run	2D ADV at WG4		Red Vectrino at WG5		Blue Vectrino at WG7	
	$\overline{u}$ (*cm/s*)	σ_u (*cm/s*)	$\overline{u}$ (*cm/s*)	σ_u (*cm/s*)	$\overline{u}$ (*cm/s*)	σ_u (*cm/s*)
N1	-6.97	21.61	-6.51	17.82	0.04	4.43
N2	-6.64	21.31	-6.47	17.76	0.02	4.90
N3	-6.36	20.71	-5.43	17.48	-0.32	5.08
N4	-6.26	21.04	-5.72	17.84	-0.32	5.11
N5	-6.52	20.77	-5.61	17.79	-0.83	5.33
N6	-7.29	21.09	-5.46	17.76	-0.13	5.49
N7	-6.70	20.85	-5.97	17.89	-0.10	5.44
N8	-6.20	21.31	-6.39	18.09	-0.77	5.43
N9	-5.72	20.99	-5.91	18.33	-0.86	5.43
N10	-6.73	20.86	-5.49	17.88	-0.93	5.44
N11	-5.46	19.59	-5.75	17.72	-0.84	5.03
N12	-6.36	20.86	-6.20	17.93	-0.28	5.01
N13	-6.91	21.11	-6.30	17.87	-0.52	5.05
N14	-7.25	20.77	-6.12	17.65	-0.38	5.18
N15	-6.80	20.63	-6.15	18.18	-0.36	5.18
N16	-7.45	20.59	-6.28	17.90	-0.21	5.16
N17	-6.14	20.49	-6.04	17.66	-1.04	5.09
N18	-7.38	20.42	-5.90	17.59	-0.91	5.11
N19	-4.73	20.03	-4.99	16.97	-0.26	5.11
N20	-4.99	20.31	-5.79	17.51	-0.54	5.26
N21	NR	NR	NR	NR	NR	NR
N22	-5.72	19.96	-6.04	17.39	-1.22	5.35
N23	-5.94	19.96	-5.67	17.56	-1.25	5.24
N24	-6.46	20.55	-6.53	17.57	-0.90	5.36
N25	-6.35	20.39	-5.55	17.50	-1.54	5.54
N26	-7.48	20.18	-6.53	17.31	-1.50	5.62
N27	-7.04	20.25	-6.61	17.75	-2.06	5.49
N28	-6.53	20.37	-5.49	17.73	-1.70	5.54
N29	-6.67	20.46	-5.84	17.63	-1.94	5.66
N30	NR	NR	NR	NR	NR	NR
Avg.	**-6.47**	**20.62**	**-5.96**	**17.72**	**-0.77**	**5.25**

NR implies "not reliable" data

Table 3.11 Mean $\overline{u}$ and standard deviation σ_u of measured cross-shore velocity u, Test R.

Run	2D ADV at WG4		Red Vectrino at WG5		Blue Vectrino at WG7	
	$\overline{u}$ (*cm/s*)	σ_u (*cm/s*)	$\overline{u}$ (*cm/s*)	σ_u (*cm/s*)	$\overline{u}$ (*cm/s*)	σ_u (*cm/s*)
R1	-6.39	20.92	-5.86	18.11	-0.78	3.52
R2	-7.34	21.01	-5.05	17.96	-0.85	3.53
R3	-7.48	21.11	-5.88	17.78	-0.52	3.69
R4	-7.58	20.64	-5.60	18.09	-1.53	3.69
R5	-7.46	20.96	-6.67	17.75	-1.74	3.82
R6	-7.07	20.86	-6.65	17.56	-1.13	3.83
R7	-9.07	21.03	-5.34	17.69	-1.34	3.72
R8	-8.55	20.78	-5.33	17.69	-1.40	3.69
R9	-7.87	21.04	-3.60	18.36	-0.81	3.68
R10	-9.01	21.14	-6.56	17.52	-1.35	3.64
R11	-6.93	20.92	-6.64	17.68	-1.29	3.54
R12	-7.14	20.76	-5.14	17.75	-0.94	3.65
R13	-7.69	21.12	-6.87	18.01	-1.44	3.56
R14	-6.79	21.16	-6.47	17.84	NA	NA
R15	-6.51	20.88	-5.89	17.94	-1.44	3.54
R16	-7.23	20.72	-5.64	17.76	-1.11	3.58
R17	-8.53	20.49	-5.58	17.70	-1.01	3.52
R18	-8.15	20.29	-6.07	17.79	-1.30	3.55
R19	-7.28	20.51	-5.60	17.77	-1.30	3.56
R20	-7.92	20.45	-6.87	17.57	-1.09	3.59
R21	-7.61	19.02	-4.12	17.69	-1.70	3.30
R22	-7.76	20.45	-6.28	17.53	-1.98	3.19
R23	-7.43	20.46	-5.46	17.65	-1.58	3.46
R24	-8.09	20.22	-6.15	17.59	NA	NA
R25	-7.61	20.03	-4.68	17.75	-1.93	3.31
R26	-8.44	20.31	-6.03	17.63	-1.50	3.35
R27	-7.02	20.33	-5.44	17.60	-0.96	3.60
R28	-7.45	20.09	-6.22	17.47	-1.53	3.45
R29	-7.53	20.01	-6.39	17.59	-1.51	3.49
R30	-7.36	20.10	-5.61	17.61	-2.14	3.49
Avg.	**-7.61**	**20.59**	**-5.79**	**17.75**	**-1.33**	**3.56**

NA implies "not available" data

Table 3.12 Mean $\overline{u}$ and standard deviation σ_u of measured cross-shore velocity u, Test C.

Run	**2D ADV at WG4**		**Red Vectrino at WG5**		**Blue Vectrino at WG7**	
	$\overline{u}$ **(*cm/s*)**	σ_u **(*cm/s*)**	$\overline{u}$ **(*cm/s*)**	σ_u **(*cm/s*)**	$\overline{u}$ **(*cm/s*)**	σ_u **(*cm/s*)**
C1	-6.60	19.93	-5.57	17.77	0.17	4.84
C2	-6.64	20.79	-6.13	17.93	-0.36	4.55
C3	-6.11	20.82	-6.19	18.09	-0.73	4.82
C4	-6.50	20.69	-5.77	17.97	-1.20	4.99
C5	-6.66	20.74	-4.26	18.00	-1.06	5.05
C6	-6.11	20.51	-4.89	17.72	-1.18	5.07
C7	-6.26	20.47	-4.60	17.87	-1.17	5.10
C8	-6.98	20.31	-5.87	17.70	-1.06	5.21
C9	-5.45	20.35	-5.41	17.77	-1.09	5.13
C10	-6.63	20.40	-4.78	17.57	-1.13	5.18
C11	-5.26	20.22	-4.46	17.66	-1.07	4.94
C12	-6.20	20.06	-4.86	17.73	-0.87	4.92
C13	-6.03	20.09	-4.79	16.55	-1.19	4.98
C14	-5.88	20.42	-4.67	15.64	-1.18	4.91
C15	-7.14	19.83	-4.50	15.91	-1.03	4.89
C16	-4.64	20.23	-4.10	15.73	-0.84	4.91
C17	-6.46	20.04	-5.07	15.67	-1.06	4.93
C18	-5.91	20.06	-4.48	15.89	-0.86	4.62
C19	-6.26	20.34	-3.58	15.77	-0.76	4.91
C20	-6.09	20.19	-5.82	16.20	-0.61	4.74
C21	-6.34	19.36	-4.39	16.18	-0.67	4.68
C22	-5.28	19.70	-4.17	16.56	-0.19	4.70
C23	-5.70	20.25	-4.45	16.68	-0.01	4.67
C24	-6.70	19.92	-4.82	16.57	-0.15	5.01
C25	-6.00	19.49	-4.40	16.58	-0.12	4.92
C26	-5.44	20.03	-4.76	16.42	-0.05	4.79
C27	-6.04	19.74	-5.30	16.91	-0.49	4.75
C28	-6.79	19.78	-3.60	16.41	-0.44	4.48
C29	-6.76	19.43	-4.19	16.33	-0.10	4.87
C30	-5.48	19.67	-5.70	16.37	-0.30	4.85
Avg.	**-6.14**	**20.13**	**-4.85**	**16.87**	**-0.69**	**4.88**

The measured values of the mean and standard deviation of the free surface elevation η and cross-shore velocity u at each location for the 30 runs in Tests N, R, and C are averaged and compared in Figure 3.1. The average values of $\bar{\eta}$ were negative (wave setdown) at WG1 to WG3 outside the surf zone and slightly negative (wave setdown) at WG4 and WG5 in the breaker zone of large waves. The average values for $\bar{\eta}$ were slightly positive (wave setup) at WG6 in the swash or inner surf zone. WG6 was situated on the crest of the barrier (swash zone) at the start of Tests N and C and subsequently located in the inner surf zone after erosion in these two tests. WG6 was located in the inner surf zone from the beginning to the end of Test R. The average values for $\bar{\eta}$ were positive (wave setup) at WG7 and WG8 in the wave transmission zone (bay) landward of the barrier. $\bar{\eta}$ in the enclosed bay increased somewhat with the increase of the barrier crest elevation where overtopped water was allowed to return seaward from the bay.

The cross-shore variation of the standard deviation σ_η at WG1 – WG8 indicated the wave height (H_{mo} = $4\sigma_\eta$) decaying landward due to wave breaking on the beach seaward of the barrier crest. The slight difference of the offshore wave heights disappeared at x = 8.0 and 9.5 m in the outer surf zone. The relatively higher $\bar{\eta}$ and smaller σ_η at WG7 and WG8 in the bay landward of the sand barrier represented the increased water level by wave overtopping and the small transmitted wave energy.

The mean cross-shore velocity $\bar{u}$ was negative due to the wave-induced offshore return current apart from slightly positive $\bar{u}$ at the beginning of Tests N and C (Tables 3.10 and 3.12) when the bay water level was increased by wave overtopping (transient water level increase). The positive value of σ_u corresponds to the intensity of the wave-induced oscillatory velocity. The return current and oscillatory velocity decreased from the breaker zone to the wave transmission zone. Sand was deposited in the bay due to the small transmitted wave energy in this experiment.

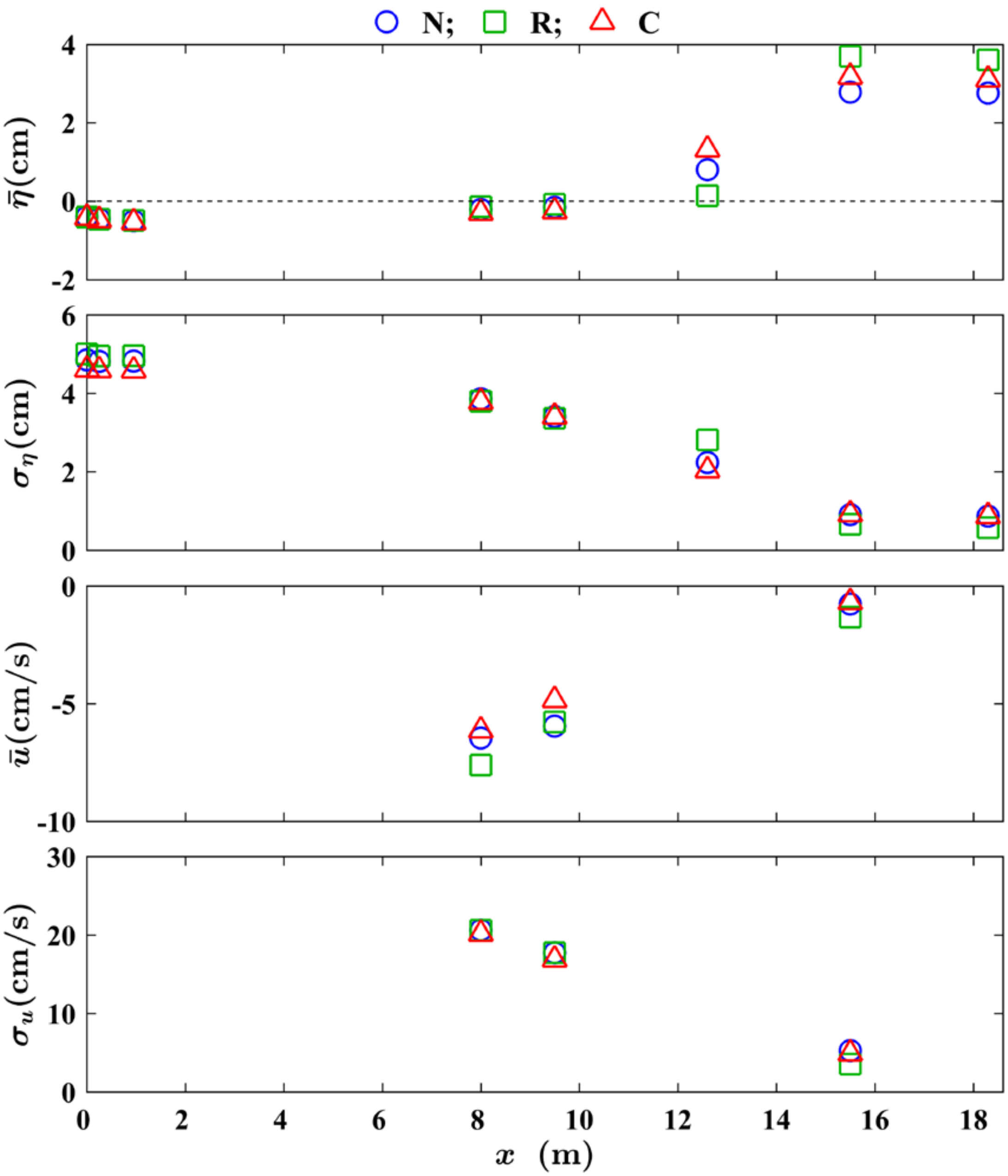

Figure 3.1 Average values of mean and standard deviation of free surface elevation η and cross-shore velocity u for 30 runs for Tests N, R, and C

3.2 Barrier Beach Profile Evolution

Figures 3.2 – 3.4 depict the measured barrier beach profiles for Tests N, R, and C at time t = 0, 2,000, 4,000, 8,000, and 12,000 s where the elevation is zero at the SWL of water depth d = 92 cm. The vertical profile changes during the 30 runs were a few centimeters in the zone of x = 5 – 8 m and more than 10 cm in the zone of x = 9 – 17 m. The entire measured profile (x = 4.5 – 18.6 m) by the laser line system is shown in the upper panel of these figures. The enlarged profile in the range of $x \approx 8 – 18$ m is shown in the lower panel.

In Test N, the sand barrier migrated landward and its crest was lowered to the SWL during t = 0 – 2,000 s (see Figure 3.2). The seaward slope of the barrier was eroded significantly and became gentler. The formation of a small step in the middle of the slope may have been resulted from wave breaking and overtopping. Most eroded sand was transported over the crest and deposited in the bay. Some eroded sand was transported offshore by the return current and deposited at the toe of the seaward slope as well as in the outer bar (x = 6 – 8 m). The landward migration of the barrier continued steadily during t = 2,000 – 12,000 s. The crest of the sand barrier was submerged at the end of Test N. Hence, the rock mound was placed on the top of the deformed sand barrier to reduce the barrier crest lowering and onshore migration for Test R.

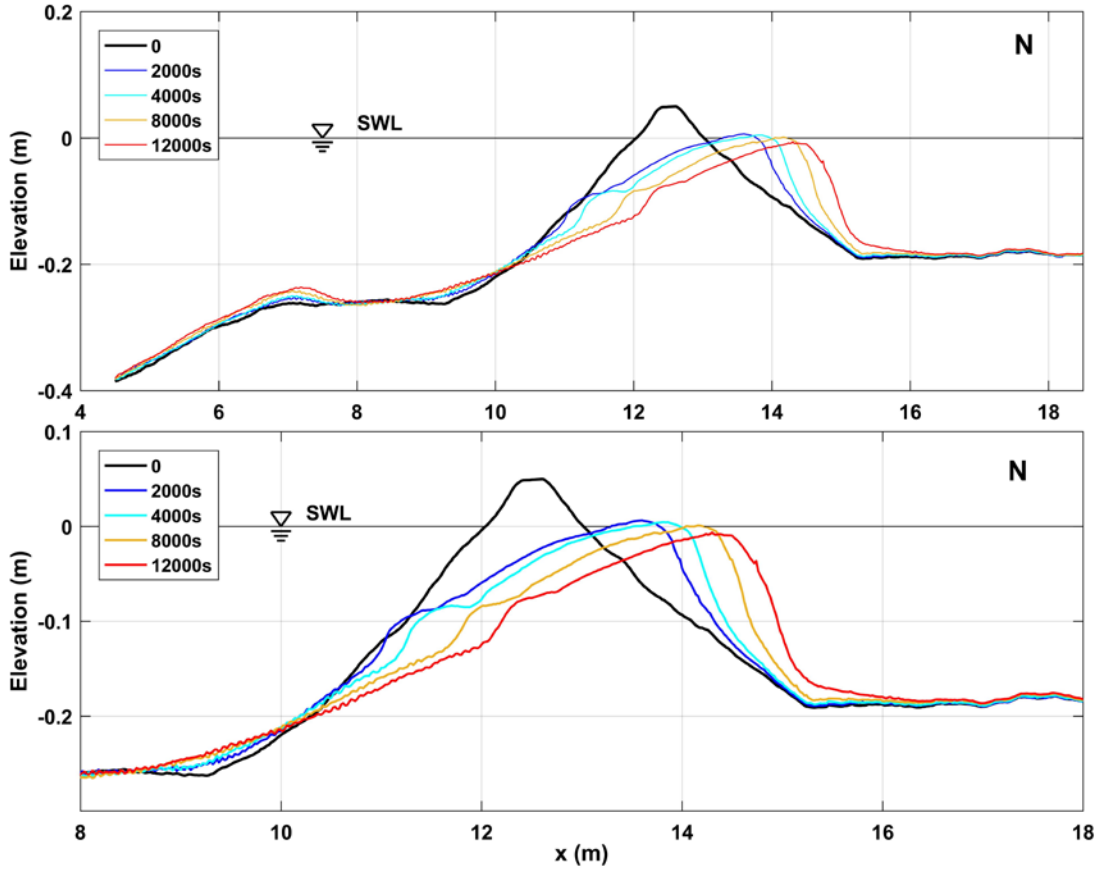

Figure 3.2 Measured profile evolution for Test N

For the rock mound R test, the measured profile evolution is depicted in Figure 3.3. The rock mound was located in the zone of x =14.02 – 14.48 m enclosed in the black line where the lower boundary is the measured sand surface before the stone placement. The mound crest was lowered noticeably during t = 0 – 2,000 s and stabilized slowly between t = 2,000 – 12,000 s. The enclosed red line indicates the upper and lower boundaries of the rock mound at the end of Test R. Erosion and accretion patterns seaward of the rock mound for Test R and the sand barrier for Test N were similar with less sand erosion in Test R. Sand accretion occurred in the bay landward of the rock mound, because of wave overtopping and onshore sand transport over, through and under the rock mound. The three-layer rock mound remained emerged at t = 12,000 s and reduced onshore movement of the sand barrier.

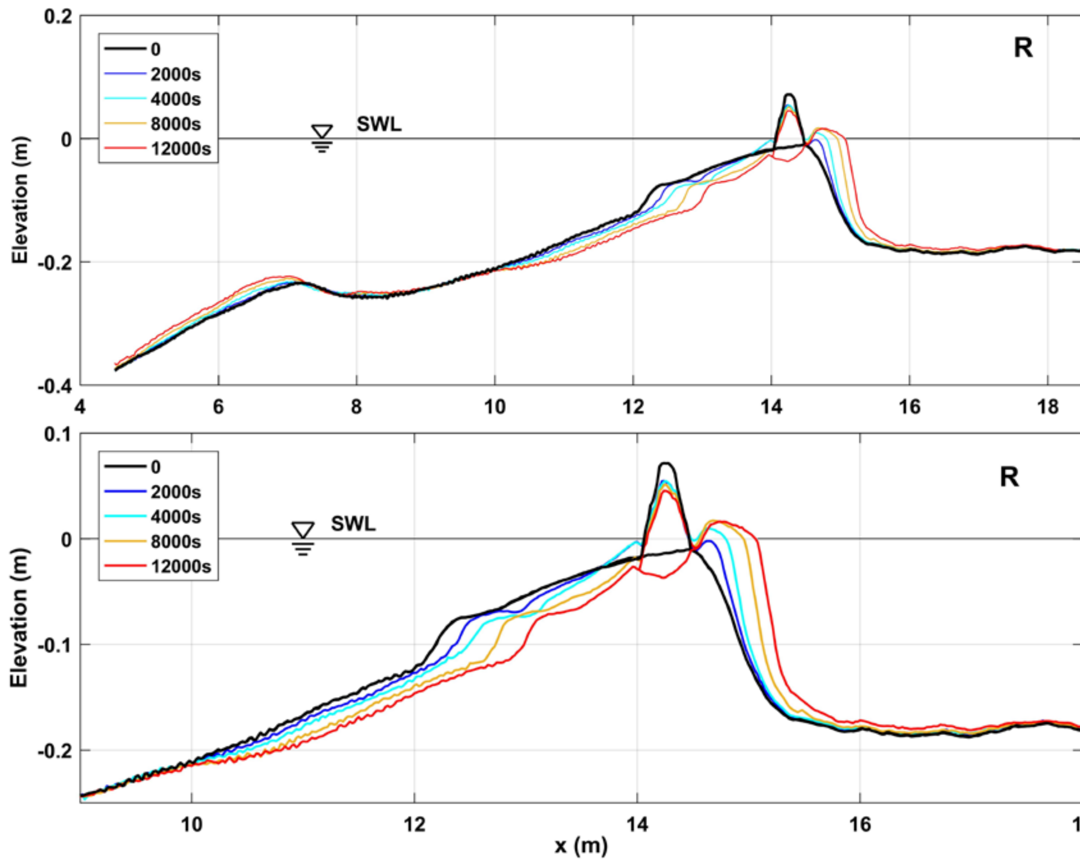

Figure 3.3 Measured profile evolution for Test R

The profile evolution of the rock cover C test is depicted in Figure 3.4. The rock cover was situated in the zone of x = 12.24 – 12.78 m enclosed in the black line where the lower boundary was the measured sand surface before the stone placement. During $t = 0 – 2{,}000$ s, the sand barrier moved onshore and the rock cover settled considerably because of onshore sand transport through and below the rock cover. The single-layer rock cover did not prevent erosion in the vicinity of the barrier crest. The enclosed red line indicates the upper and lower boundaries of the rock cover at the end of Test C. The rock cover settled and dispersed as sand particles between and below the green stones were eroded by wave action.

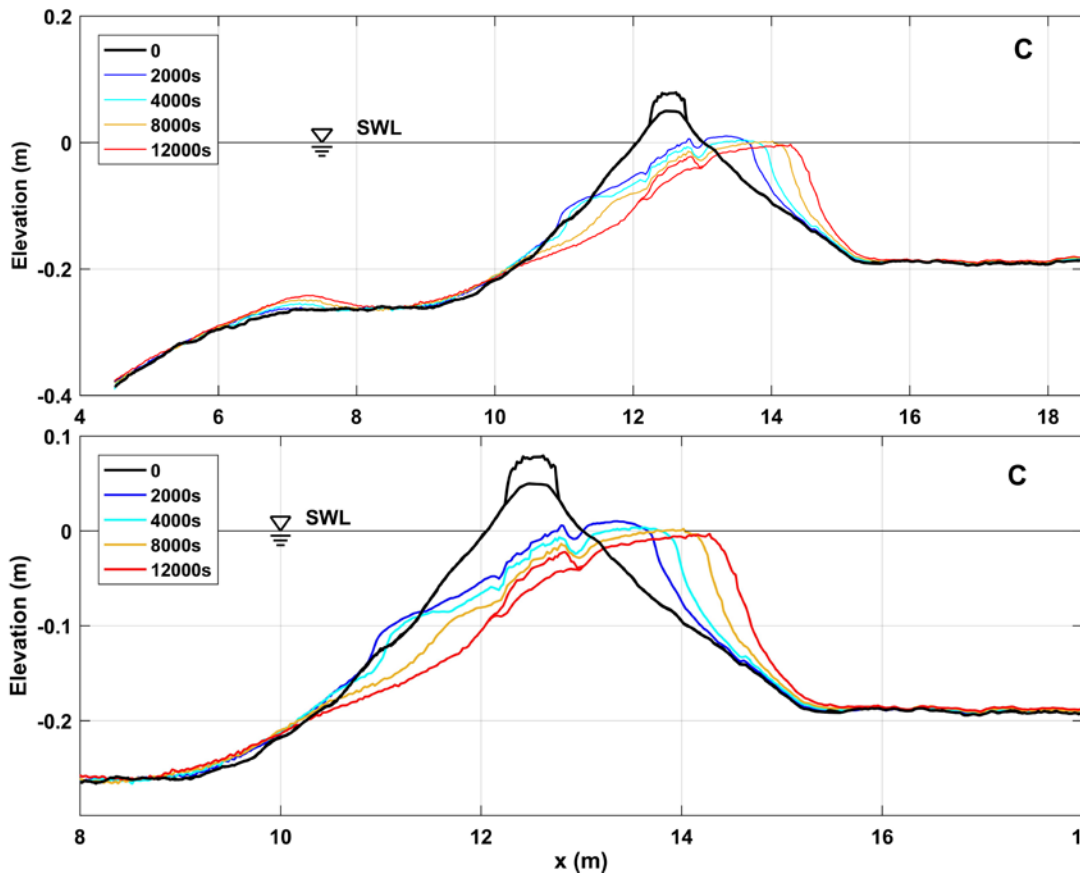

Figure 3.4 Measured profile evolution for Test C

The comparisons of the measured profiles at t = 0, 2,000, 4,000, 8,000, 12,000 s of Tests C and N are presented in Figure 3.5. The onshore movement and crest lowering of the sand barrier for the two tests were very similar. However, the single-layer rock cover slightly reduced the landward migration of the sand barrier for the entire duration even after the rock cover was well submerged.

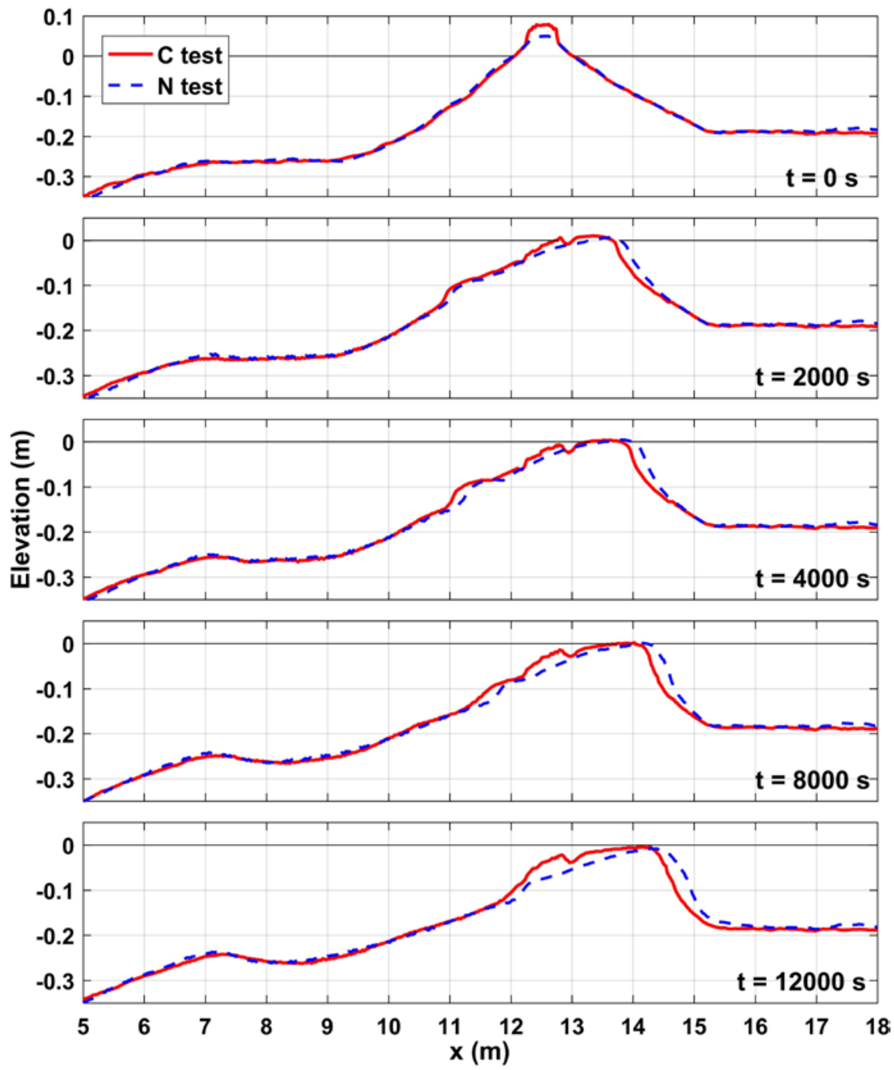

Figure 3.5 Comparison of measured profile evolution for Tests C and N at t = 0, 2,000, 4,000, 8,000, and 12,000 s

3.3 Sediment Volume Budget

The sediment budget is examined by calculating the volumetric changes of the measured profiles from the initial profile at t = 0 in the range of x = 4.5 – 18.6 m. Tables 3.13 – 3.15 tabulate the cumulative deposited (V_d), eroded (V_e), and lost ($V_l = V_e - V_d$) sediment volumes per unit alongshore width at t = 2,000, 4,000, 8,000, and 12,000 s for Tests N, R, and C. For Test N with no structure, the deposited and eroded sand volumes should be equal, $V_d = V_e$. However, the lost sand volume V_l increased from 0.00096 m^2 at t = 2,000 s to 0.0063 m^2 at t = 12,000 s. For Test R, the initial cross-sectional area of the rock mound (no sand inside) was 0.023 m^2 and the stone porosity was 0.44. Thus, the pore area was 0.010 m^2. The measured profile corresponded to the sand or stone surface elevation. Sand volume inside the rock mound was not measured. The lost sand volume was less than 0.005 m^2, some of which may have been inside the rock mound. For Test C, the initial cross-sectional area of the rock cover was 0.014 m^2 with the pore area of 0.006 m^2. The lost sand volume was about 0.007 m^2 at t = 12,000 s.

In order to quantitatively evaluate the effectiveness of the rock mound and cover, Figure 3.6 compares the temporal variations of the eroded volume V_e per unit width for the three tests. The three-layer rock mound reduced the barrier erosion by a factor of about 2. The erosion reduction was 10 – 20% for the single-layer rock cover. Sediment (sand and stone) erosion and accretion decreased for Tests R and C in comparison to Test N, indicating that the rock structure provided partial protection for the sand barrier.

After Tests R and C, the rock structure was removed and the profile was measured as shown in Figure 3.7. Sand attached to the stones was collected and placed in the zone of the rock structure and smoothed before the profile measurement (Figure 3.8). The cumulative deposited, eroded, and lost sand volumes during t = 0 – 12,000 s for Tests N, R, and C after removing the rock structure are listed in Table 3.16. The reduction of the eroded and deposited sand volumes was noticeable for Test R, comparing the values in Tables 3.14 and 3.16 where the stone volume is the noticeable fraction of the sediment volume in Table 3.14.

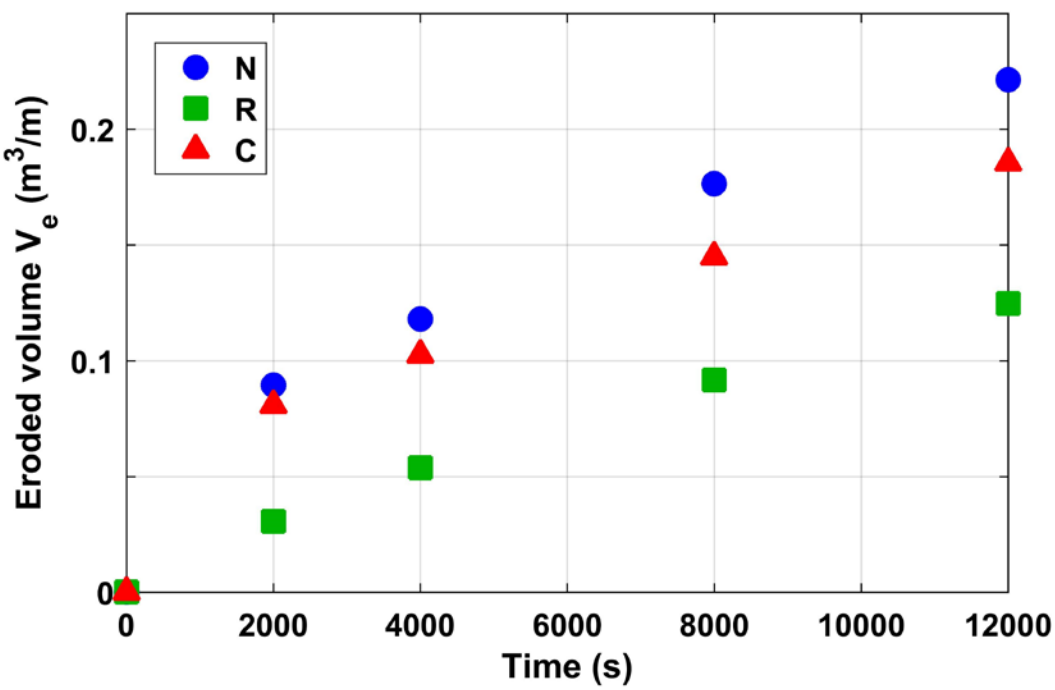

Figure 3.6 Temporal variations of eroded volume V_e per unit width for Tests N, R, and C

Table 3.13 Cumulative deposited sediment volume V_d, eroded sediment volume V_e, and lost sediment volume V_l after 5, 10, 20, and 30 runs, Test N.

Time Interval	**Run**	**Sediment Volume per Unit Width (m^3/m)**			
		V_d	V_e	V_l	V_l/V_e
t = 0 – 2,000 s	5	0.0885	0.0894	0.00096	0.011
t = 0 – 4,000 s	10	0.1162	0.1180	0.0018	0.015
t = 0 – 8,000 s	20	0.1724	0.1764	0.0040	0.023
t = 0 – 12,000 s	30	0.2150	0.2213	0.0063	0.028

Table 3.14 Cumulative V_d, V_e, and V_l after 5, 10, 20, and 30 runs, Test R (with rock).

Time Interval	**Run**	**Sediment Volume per Unit Width (m^3/m)**			
		V_d	V_e	V_l	V_l/V_e
t = 0 – 2,000 s	5	0.0295	0.0305	0.00099	0.032
t = 0 – 4,000 s	10	0.0516	0.0537	0.0021	0.039
t = 0 – 8,000 s	20	0.0870	0.0917	0.0047	0.051
t = 0 – 12,000 s	30	0.1341	0.1247	-0.0095	-0.076

Table 3.15 Cumulative V_d, V_e, and V_l after 5, 10, 20, and 30 runs, Test C (with rock).

Time Interval	**Run**	**Sediment Volume per Unit Width (m^3/m)**			
		V_d	V_e	V_l	V_l/V_e
t = 0 – 2,000 s	5	0.0783	0.0808	0.0026	0.032
t = 0 – 4,000 s	10	0.0965	0.1025	0.0059	0.058
t = 0 – 8,000 s	20	0.1374	0.1449	0.0075	0.052
t = 0 – 12,000 s	30	0.1788	0.1855	0.0068	0.037

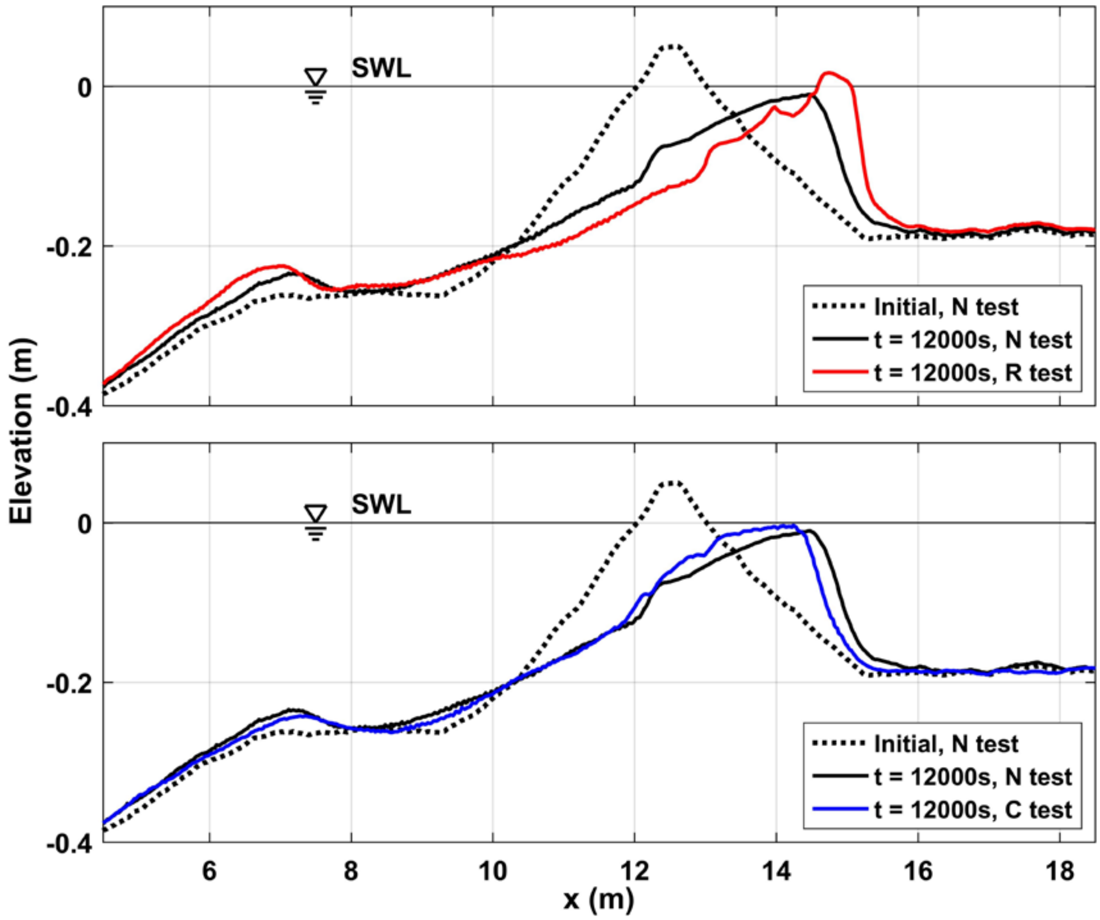

Figure 3.7 Initial and final profiles for Test N as well as final profiles for Tests R and C after removing stones

Table 3.16 Deposited sand volume V_d, eroded sand volume V_e, and lost sand volume V_l during t = 0 – 12,000 s for Tests N, R, and C without stones.

Time Interval	Test	Sediment Volume per Unit Width (m^3/m)			
		V_d	V_e	V_l	V_l/V_e
t = 0 – 12,000 s	N	0.2150	0.2213	0.0063	0.028
t = 0 – 12,000 s	R	0.1228	0.1303	0.0075	0.058
t = 0 – 12,000 s	C	0.1774	0.1851	0.0077	0.042

(a) Test R with and without rock mound

(b) Test C with and without rock cover

Figure 3.8 Initial and final rock structures for Tests R and C as well as smooth sand surface after stone removal at the end of two tests

3.4 Rock Settlement and Spreading

Settlement and dispersion of the rock structures were observed in Tests R and C, as shown in Figure 3.8. The upper and lower bounds of the rock mound and cover at t = 0 and 12,000 s for these two tests are depicted again in Figure 3.9. For Test R, the maximum crest settlement of the rock mound was 2.6 cm and the maximum bottom settlement was 2.2 cm. The geometry of the rock mound did not change much. For Test C, the bottom settlement was up to 11.7 cm and the large settlement is an important design factor. The rock cover settled downward considerably and became elongated horizontally after 30 runs.

Figure 3.10 shows the rock thickness at the beginning and end of Tests R and C. The three-layer rock mound of Test R did not deform much and maintained most of its thickness. The single-layer rock cover of Test C spread laterally and the average rock thickness decreased from 2.8 cm at t = 0 to 1.7 cm at t = 12,000 s. The green stones of 3.52-cm nominal diameter did not move under wave action but dispersed because of the movement of sand particles in the vicinity of each stone. Sand particles among the dispersed stones became exposed to direct wave action, causing onshore and offshore sand transport by wave action. The single-layer rock cover lost its protective function because of intense sand movement.

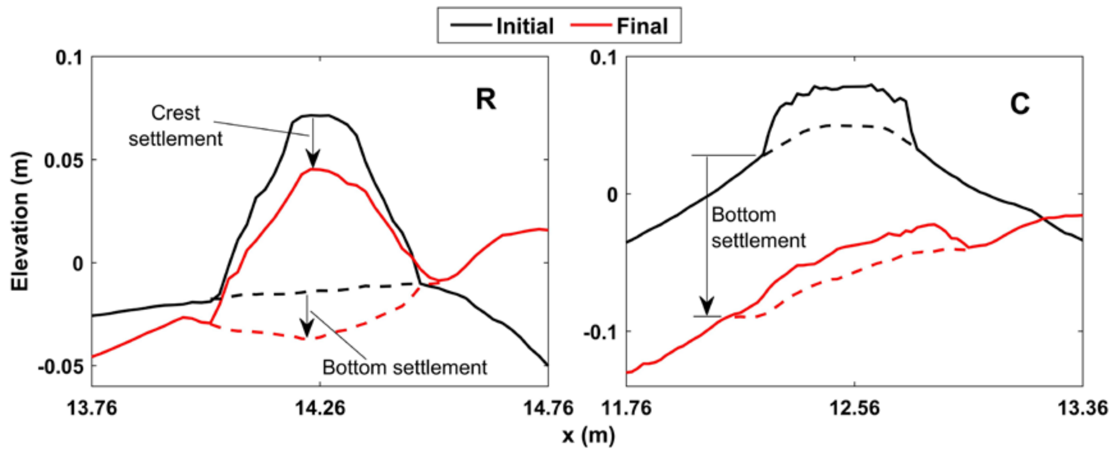

Figure 3.9 Settlement of stone surface and sand surface from time $t = 0$ to $t =$ 12,000 s for Tests R and C

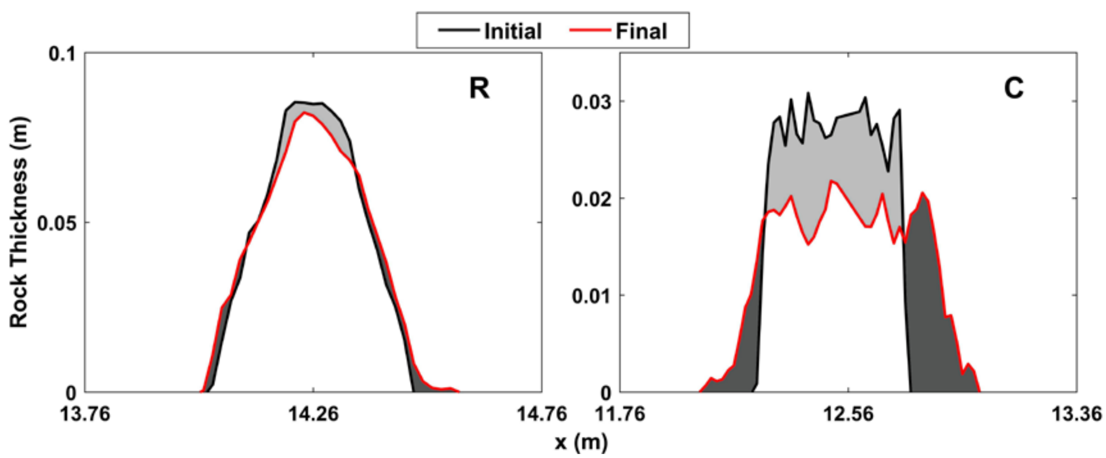

Figure 3.10 Spreading of stones from time $t = 0$ to $t = 12{,}000$ s for Tests R and C

Chapter 4

NUMERICAL MODEL

The cross-shore numerical model CSHORE was extended to a rock structure with no filter between the structure and bottom sand. This chapter concisely explaines the components and updates of the numerical model used in this study and summaries input parameters to CSHORE for the three laboratory tests. The numerical model was described in detail in the review paper of Kobayashi (2016).

4.1 Cross-shore Model (CSHORE)

The version of CSHORE used in this study included the following components: a combined wave and current model based on time-averaged continuity, momentum, wave energy, and roller energy equations; a sediment transport model for bed and suspended load coupled with the continuity equation of bottom sediment; a permeable layer model for porous flow; and a probabilistic swash model on impermeable (fine sand) and permeable (stone) bottoms. Kobayashi and Kim (2017) proposed a simple model to compute sand transport on and inside a stone structure placed on a fixed filter. Their model based on the conservation of sand volume was extended to the case of no filter, underlying sand erosion, and stone settlement. Stone dispersion was neglected. Their model included the sand transport reduction factor as a function of the porous layer thickness. This factor caused too much reduction of onshore sand transport over and through the rock mound for Test R and the rock cover for Test C. The reduction factor was omitted for the present case of no filter and intense sand transport.

The explanation of CSHORE above is limited to the seaward wet zone and the wet and dry zone above the SWL. Kobayashi et al. (2013) extended CSHORE to the landward wet zone to predict the damage and wave transmission of reef breakwaters. Transmitted waves were assumed to propagate landward at the landward boundary. The extended CSHORE was applied to predict the damage and wave transmission of low-crested stone structures under normally and obliquely incident irregular waves (Garcia and Kobayashi 2015). These studies were limited to stone structures on fixed bottoms in laboratories. Their extended CSHORE was also applied to predict wave overtopping and sand overwash of a barrier beach between the Atlantic Ocean and Rehoboth Bay in Delaware during Hurricane Sandy in 2012 (Kobayashi and Zhu 2017). The paved road on the barrier beach was neglected in the computation. Observed extensive sand overwash was predicted but no quantitative comparison was made. The CSHORE computation in this study combined the options of sand transport over and through a rock structure and wave overtopping and transmission of a barrier beach and a bay.

4.2 CSHORE Input

The measured initial profiles of the stone and sand bottoms in the computation domain of $0 \leqslant x \leqslant 18.6$ m in Figure 2.2 were specified as the initial bottom profiles at time $t = 0$ for Tests N, R, and C, denoted as z_b. The measured sand surface elevation before the stones placement at $t = 0$ was specified as input for Tests R and C, denoted as z_p. The elevation difference was the initial thickness of the rock layer, $h_p = z_b - z_p$, where z_b and z_p are respectively the upper and lower boundaries of the rock structure. The nodal spacing was 2 cm. The characteristics of sand and stones used in the experiment are tabulated in Table 4.1. The sand was characterized by its median diameter, fall velocity, specific gravity, and porosity. The stone porosity was 0.44 for both blue and green stones. The nominal diameter of the combined blue and green stones was 3.65 cm for Test R. The nominal diameter of the green stone was 3.52 cm for Test C. The measured values of $\bar{\eta}$, H_{mo}, T_p at $x = 0$ for 30 runs in each test lasting 12,000 s was specified as the seaward boundary conditions. The still water depth below the SWL was 83 cm at $x = 0$ for the three tests. The measured values of $\bar{\eta}$ at WG8 ($x = 18.3$ m) were specified as input as the landward boundary condition where the measured water level in Rehoboth Bay was used by Kobayashi and Zhu (2017).

The input parameters for CSHORE listed in Table 4.1 were taken as standard values except for the bed load parameter B (Kobayashi 2016) and the suspended load parameter a_o associated with wave overtopping (Figlus et al. 2011). The standard value $B = 0.002$ could not predict sufficient onshore barrier migration in the outer surf zone at elevation between -0.2 and -0.1 in Figures 3.2 – 3.4. CSHORE predicts onshore bed load transport but onshore bed load is larger in this experiment than in the previous experiments conducted in the same wave flume (e.g., Yuksel and Kobayashi 2020). This is probably because the sand barrier was created by moving sand offshore in Figure

2.1, from the end of the wave flume ($x \approx 18$ – 20 m) to the middle area ($x \approx 10$ – 15 m). On the other hand, the parameter a_o of the order of 1.0 increases onshore suspended sand transport by wave overtopping of the barrier crest. The two parameters were calibrated together and the calibrated value were B = 0.01 and a_o = 1.8. The agreement with the data was similar for a_o = 1.0 – 2.0 and the choice of a_o = 1.8 was based on numerical consistency for the entire duration of 12,000 s.

Table 4.1 CSHORE input parameters and sediment characteristics.

Category	Parameters	Value	Description
Input (standard)	Δx	0.02 m	cross-shore nodal spacing
	γ	0.6	breaker ratio parameter
	f_{b_sand}	0.015	sand bottom friction factor
	f_{b_stone}	0.05	stone bottom friction factor
	e_B	0.005	suspension efficiency due to wave breaking
	e_f	0.01	suspension efficiency due to bottom friction
	a	0.2	suspended load parameter
	$\tan\phi$	0.63	sediment limiting slope
Input (calibrated)	B	0.01	bed load parameter
	a_o	1.8	suspended load parameter associated with wave overtopping
Sand	d_{50}	0.18 mm	median sand diameter
	ω_f	2.0 cm/s	fall velocity
	s	2.6	specific gravity
	n_{p_sand}	0.4	porosity of sand
Stone	D_{n50_c}	3.65 cm	nominal diameter of the combined blue and green stones for Test R
	D_{n50_g}	3.52 cm	nominal diameter of the green stone for Test C
	n_{p_stone}	0.44	porosity of stone
	N_c	0.7	critical stability number of stone

Chapter 5

COMPARISON WITH DATA

The small-scale laboratory tests examined the effectiveness of a rock structure in reducing the migration and crest lowering of a sand barrier under limited conditions. The measurement on the barrier crest was limited to one wave gauge and the rate of wave overtopping could not be estimated. In this chapter, the extended CSHORE was compared with the three tests and used to predict hydrodynamic and sediment transport variables that were not measured in the experiment. Barrier profile evolution including eroded sediment volume was compared with the measured data to assess the option of no filter between the structure and bottom sand in the model CSHORE.

5.1 Cross-shore Wave Transformation

The computed and measured cross-shore variations of the mean and standard deviation of the free surface η and horizontal velocity u for Tests N, R, and C are compared for a set of 10 runs in Figures 5.1 – 5.9. The hydrodynamic variables did not change much during t = 0 – 4,000, 4,000 – 8,000, and 8,000 – 12,000 s except for some initial runs in the first set of the three tests. The mean water level $\bar{\eta}$ is the sum of the mean water depth and bottom (stone and sand) elevation (negative below the SWL). The averaging of the hydrodynamic variables in the wet and dry zone was performed for the wet duration only. The initial emerged sand barrier for Tests N and C was in the zone of x = 12.04 – 13.02 m and the barrier crest was lowered and moved onshore ending at $x \approx 14.3$ m. The rock mound for Test R was located in the zone of x = 14.02 – 14.48 m and the rock cover for Test C was placed between x = 12.24 – 12.78 m (Figures 3.2 – 3.4). Fluctuations of the computed $\bar{\eta}$ near and on the barrier crest for Tests N and C were caused by numerical difficulty dealing with small water depth or emergence. The values of $\bar{\eta}$ in the bay (landward of the barrier crest) were predicted well partly because of the use of measured $\bar{\eta}$ at WG8 (x = 18.3 m) as the landward boundary condition. The standard deviation σ_η related to the local wave height was underpredicted near the barrier crest and in the bay area ($x \approx 12$ – 18.6 m). The mean velocity $\bar{u}$ was negative (offshore) except for the noticeably positive $\bar{u}$ caused by wave overtopping of the barrier crest for Tests N and C or the rock mound for Test R. The standard deviation σ_u representing the oscillatory wave velocity was reduced considerably by the sand barrier but few fluctuations appeared on the rock cover at the beginning of Test C before the rock cover settlement (Figure 3.4).

The model CSHORE predicted these hydrodynamic variables within errors of approximately 20% except in the zone landward of the barrier crest. Wave transmission is sensitive to the crest elevation, width, and material (sand or stone) (e.g., Garcia and Kobayashi 2015). The hydrodynamic variables in the wave transmission zone were affected by the accuracy of the predicted barrier profile evolution.

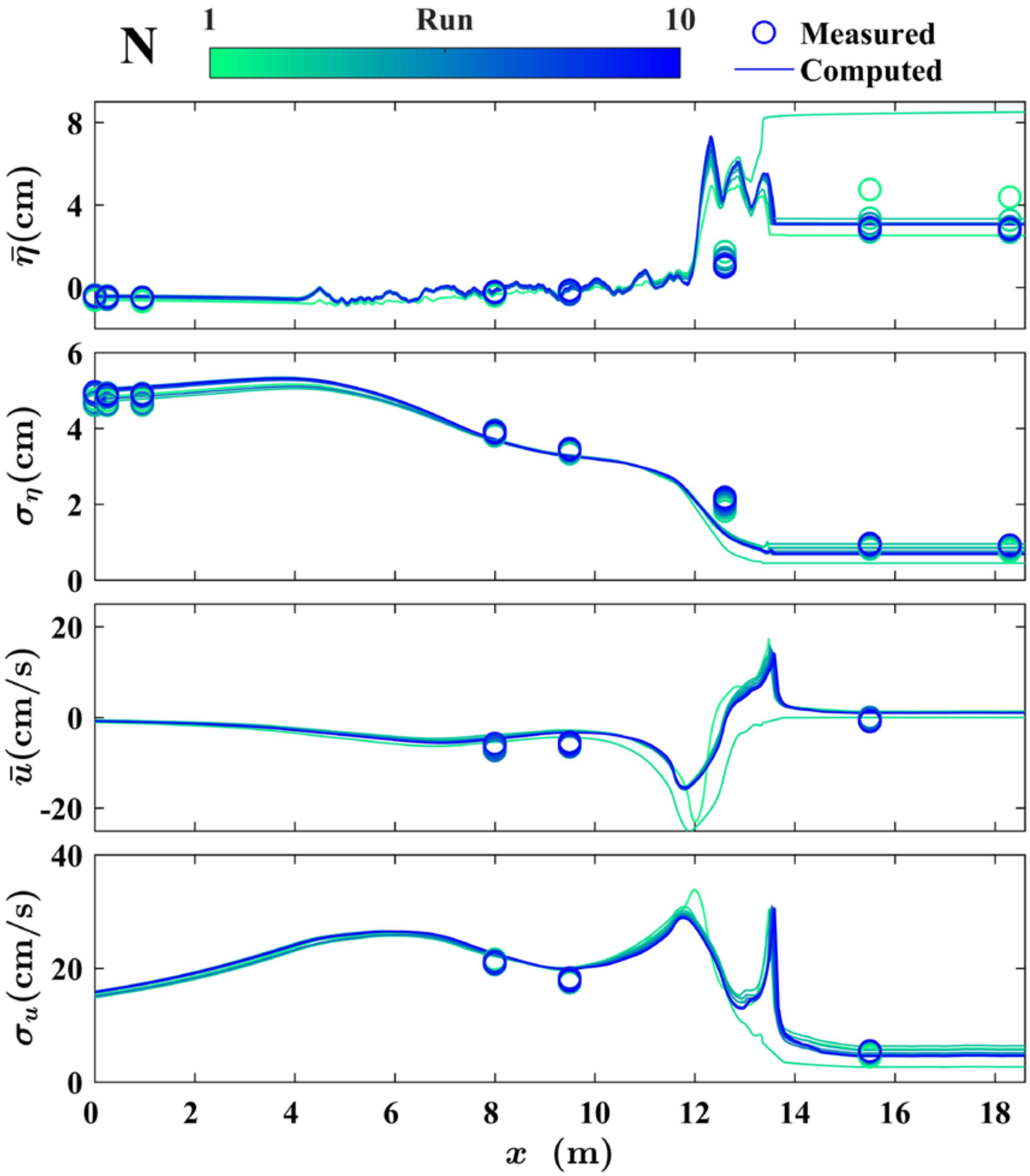

Figure 5.1 Computed and measured mean and standard deviation of free surface elevation η and horizontal velocity u for 10 runs during t = 0 – 4,000 s in Test N

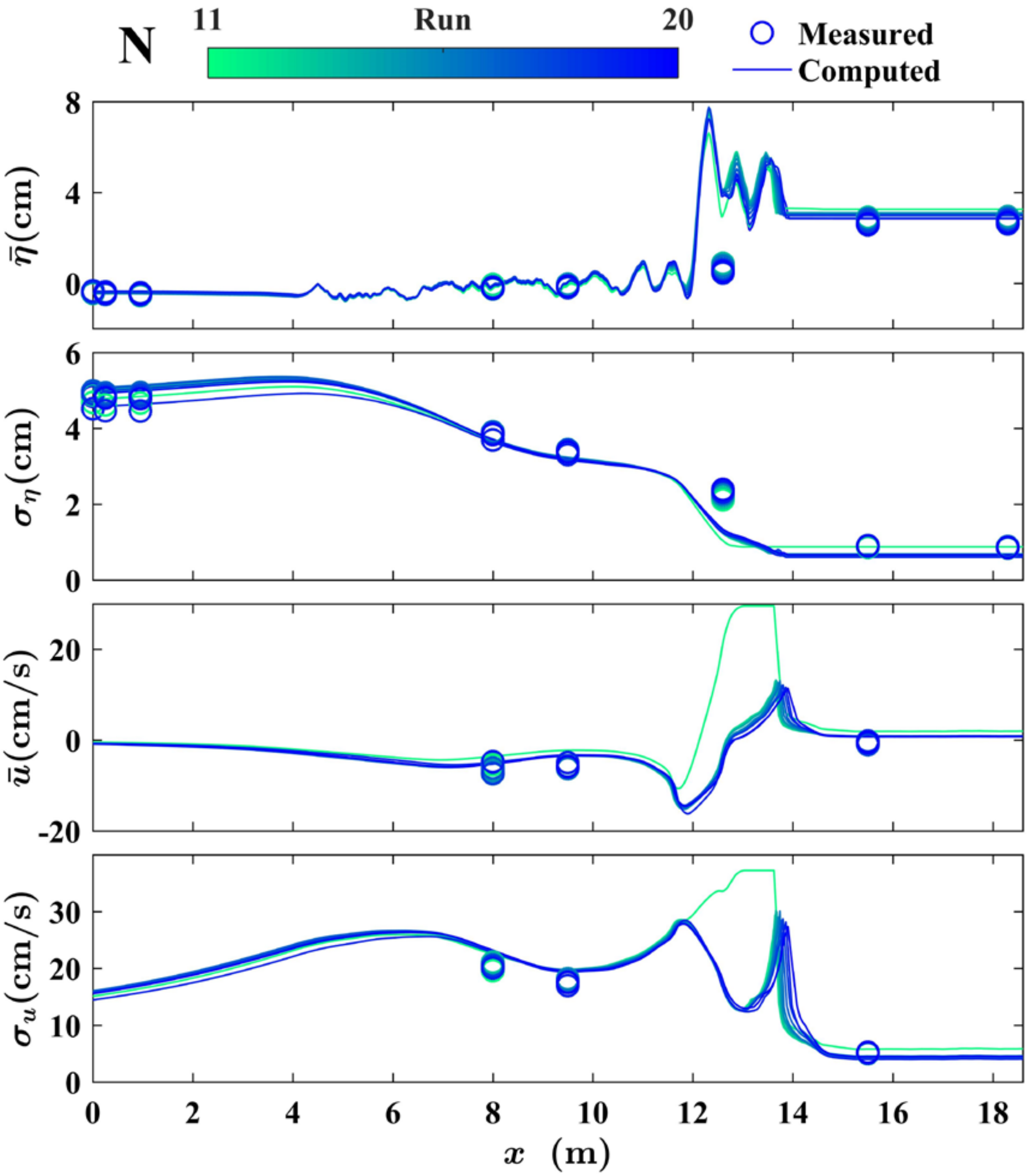

Figure 5.2 Computed and measured mean and standard deviation of η and u for 10 runs during t = 4,000 – 8,000 s in Test N

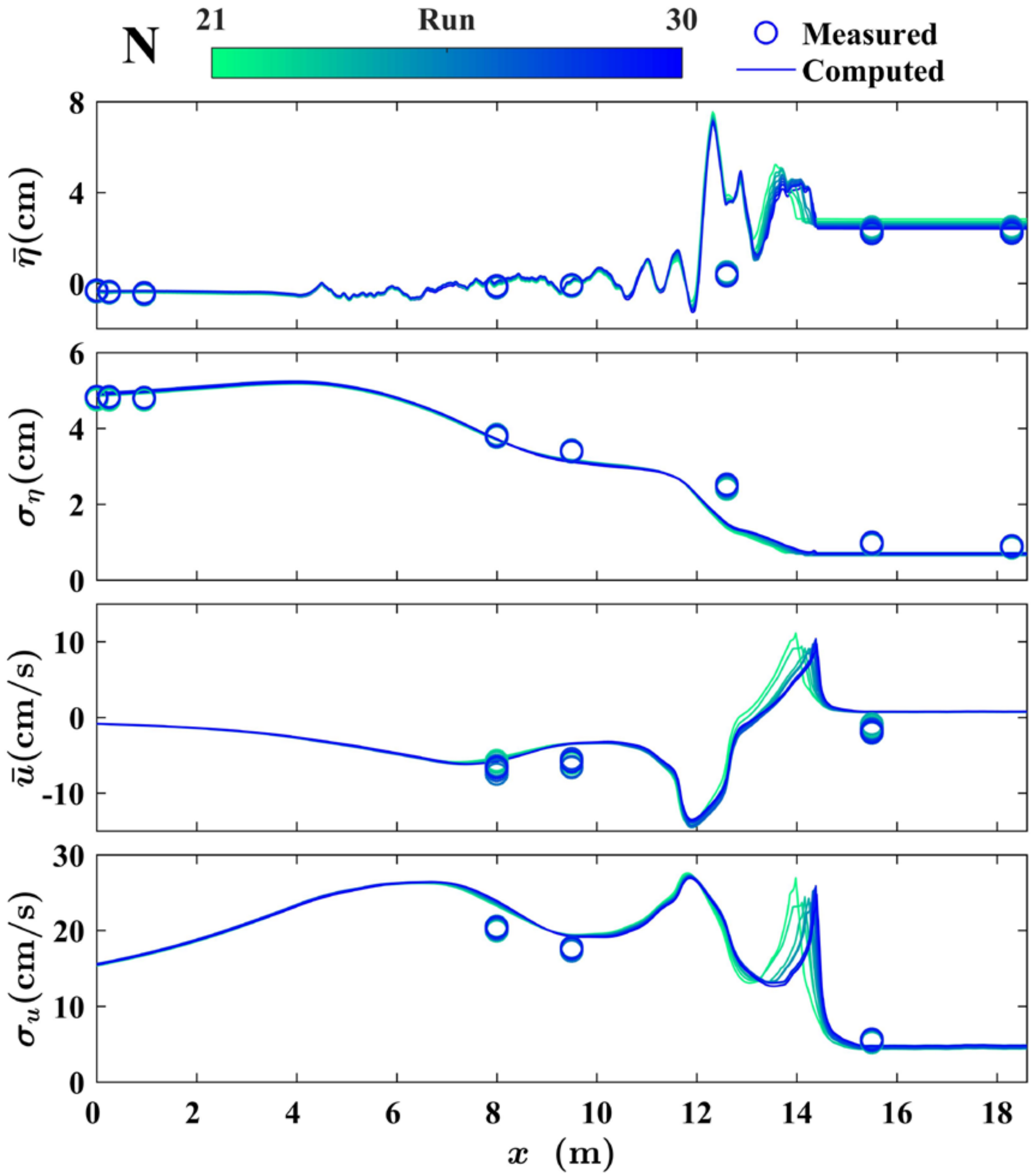

Figure 5.3 Computed and measured mean and standard deviation of η and u for 10 runs during t = 8,000 – 12,000 s in Test N

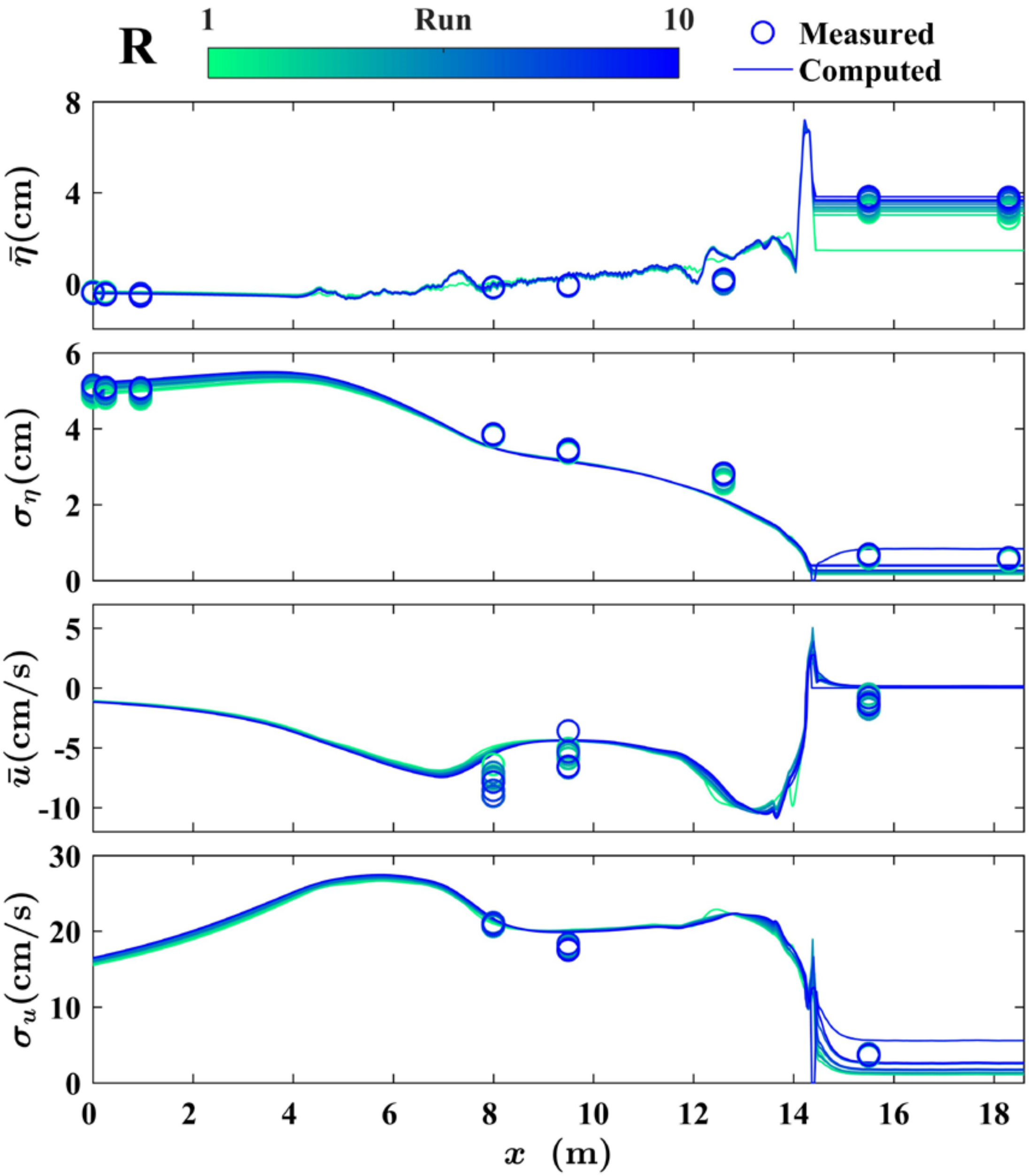

Figure 5.4 Computed and measured mean and standard deviation of η and u for 10 runs during t = 0 – 4,000 s in Test R

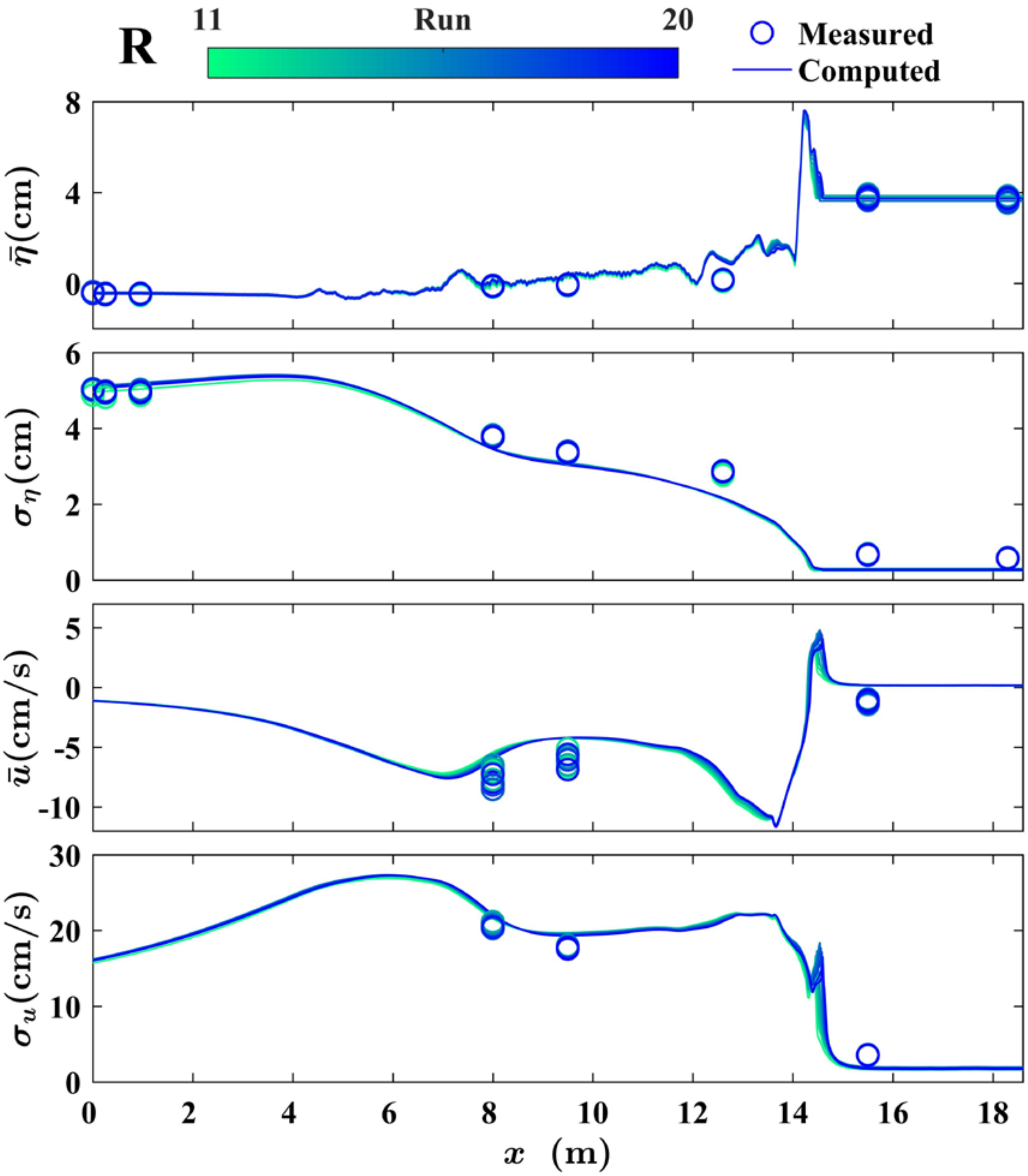

Figure 5.5 Computed and measured mean and standard deviation of η and u for 10 runs during t = 4,000 – 8,000 s in Test R

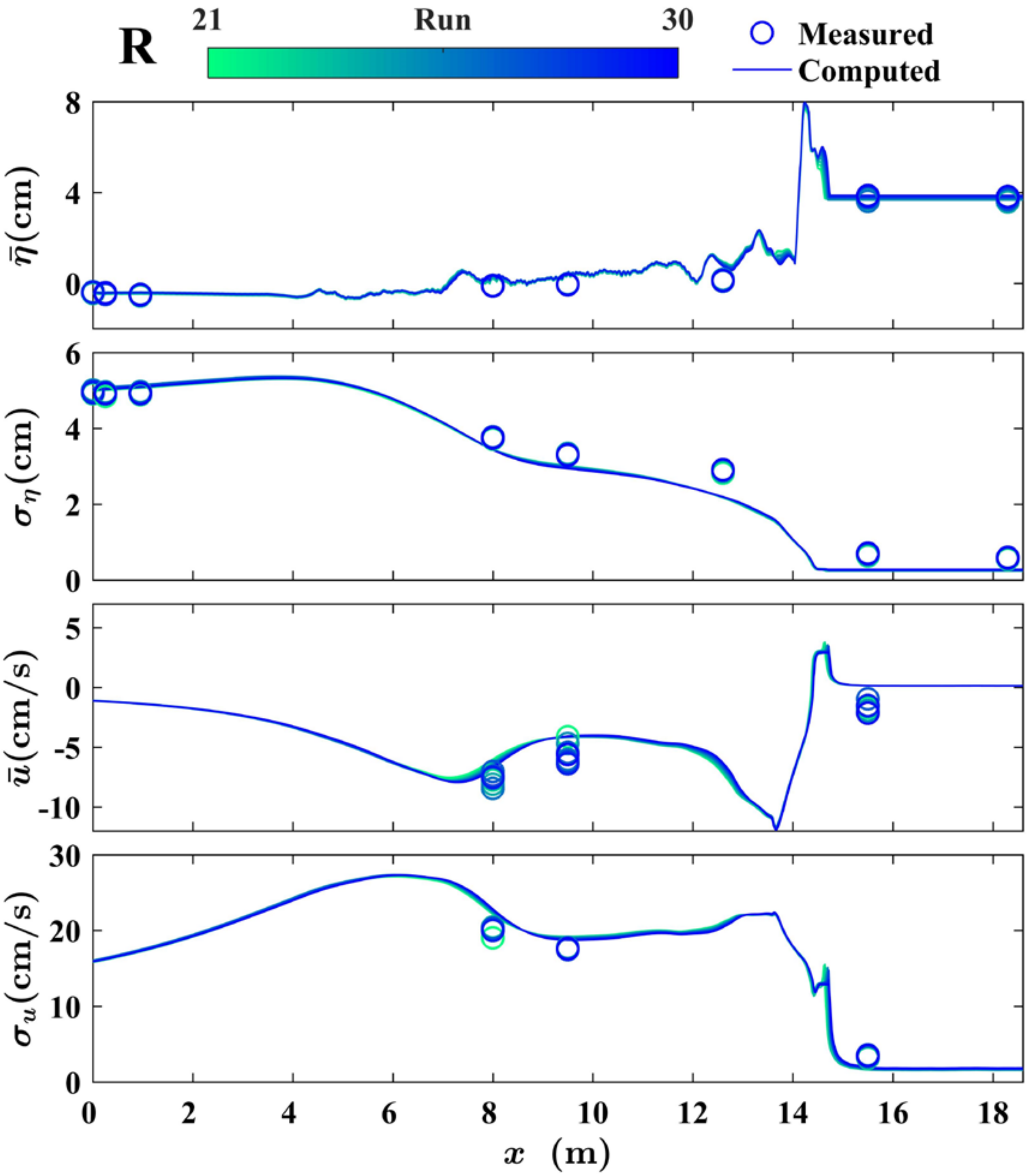

Figure 5.6 Computed and measured mean and standard deviation of η and u for 10 runs during t = 8,000 – 12,000 s in Test R

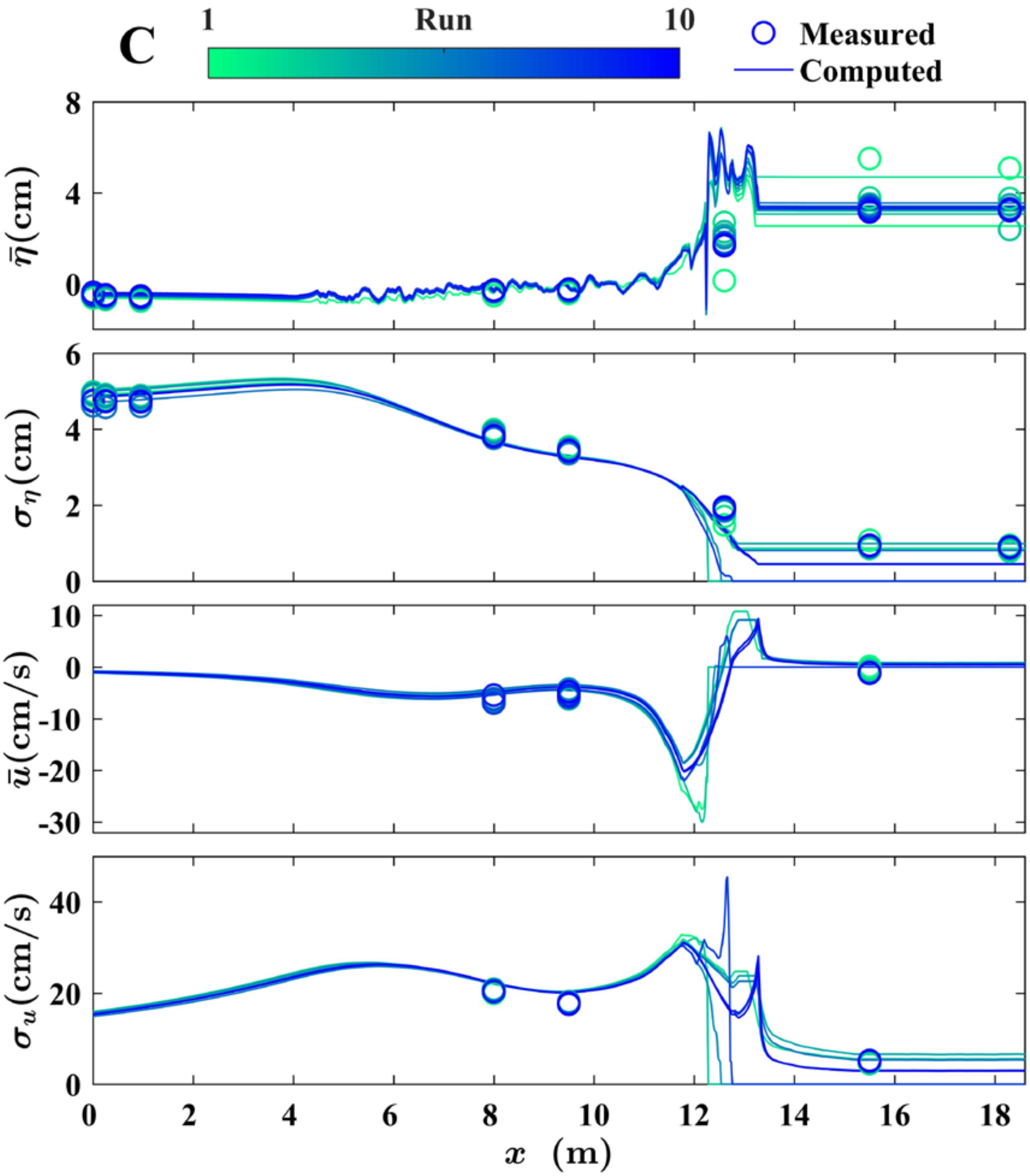

Figure 5.7 Computed and measured mean and standard deviation of η and u for 10 runs during t = 0 – 4,000 s in Test C

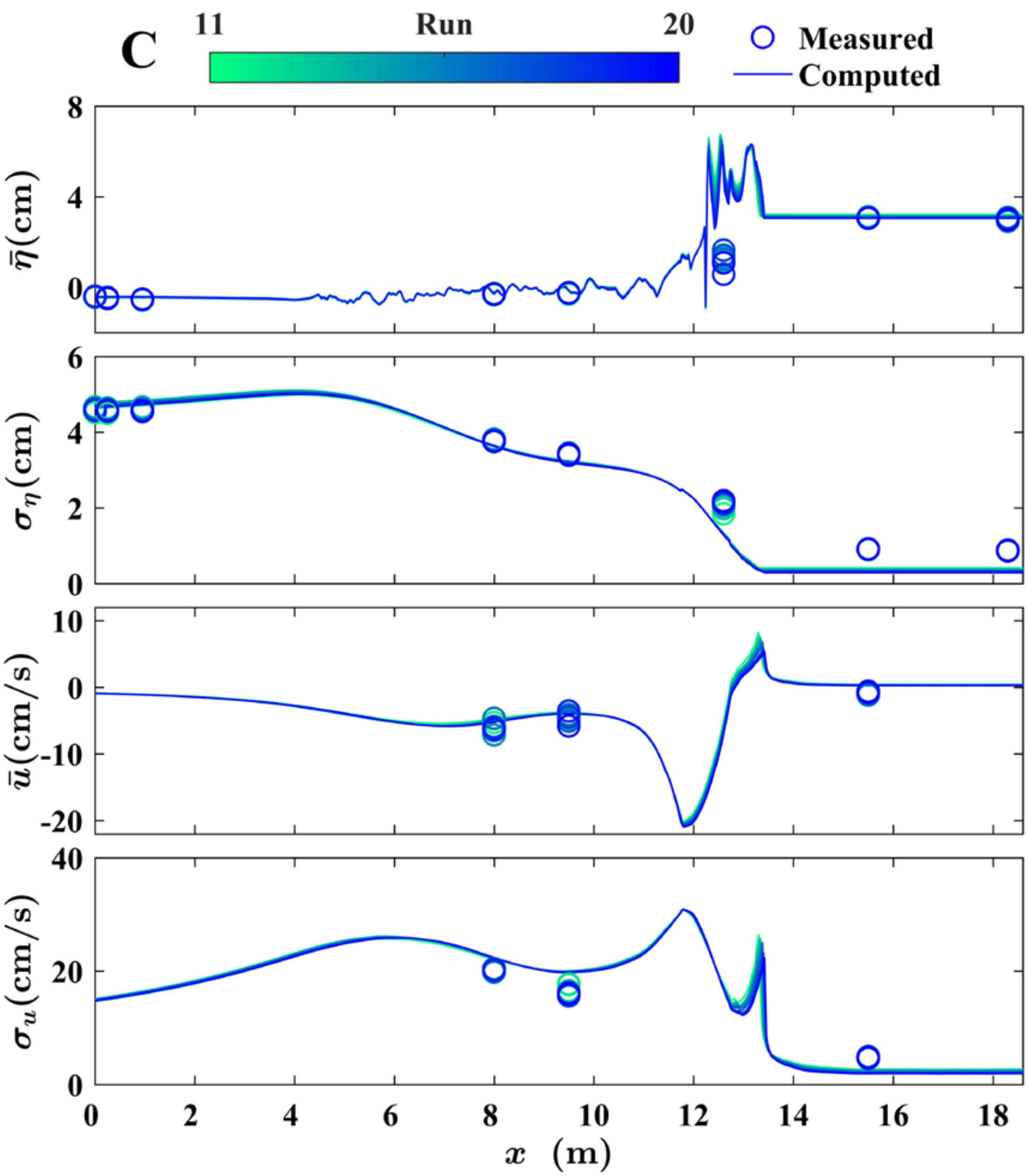

Figure 5.8 Computed and measured mean and standard deviation of η and u for 10 runs during t = 4,000 – 8,000 s in Test C

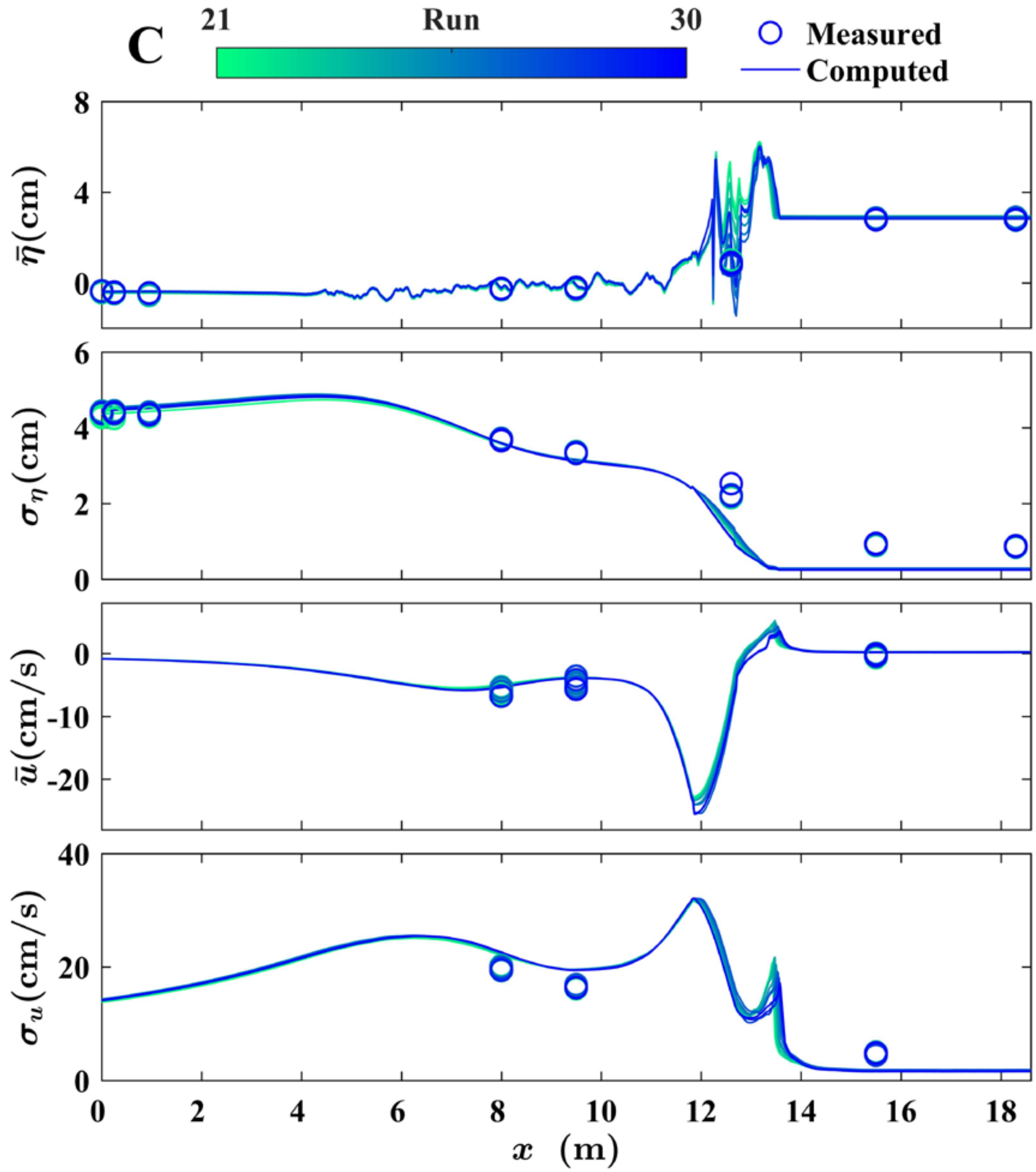

Figure 5.9 Computed and measured mean and standard deviation of η and u for 10 runs during t = 8,000 – 12,000 s in Test C

5.2 Barrier Profile Evolution and Eroded Sediment Volume

The measured and computed barrier profiles at time t = 2,000, 4,000, 8,000, 12,000 for Tests N, R, and C are compared in Figures 5.10 – 5.12. The initial profile at t = 0 is plotted in each figure to indicate the degree of the profile evolution. The crest of the computed profile in Test N developed a secondary crest because of two peaks of the computed cross-shore sand transport rate on the barrier crest where the computed sediment transport rates were presented in the next section. The rock mound in Test R was located in the zone of x = 14.02 – 14.48 m. The eroded profile seaward of the rock mound was predicted fairly. Accretion landward of the rock mound was predicted but the accretional profile did not extent landward sufficiently, perhaps because of the underprediction of transmitted waves in Figures 5.4 – 5.6. The rock cover in Test C was located in the zone of x = 12.24 – 12.78 m. The settlement of the rock cover was underpredicted because CSHORE did not account for the stone spreading and sand exposure. The discrepancy of the accretional profile landward of the rock cover is similar to that for Test R. Transmitted waves in Figures 5.7 – 5.9 were underpredicted for Test C as well. The simple hydrodynamic model for transmitted waves by Kobayashi et al. (2013) may need to be modified for narrow sand barriers.

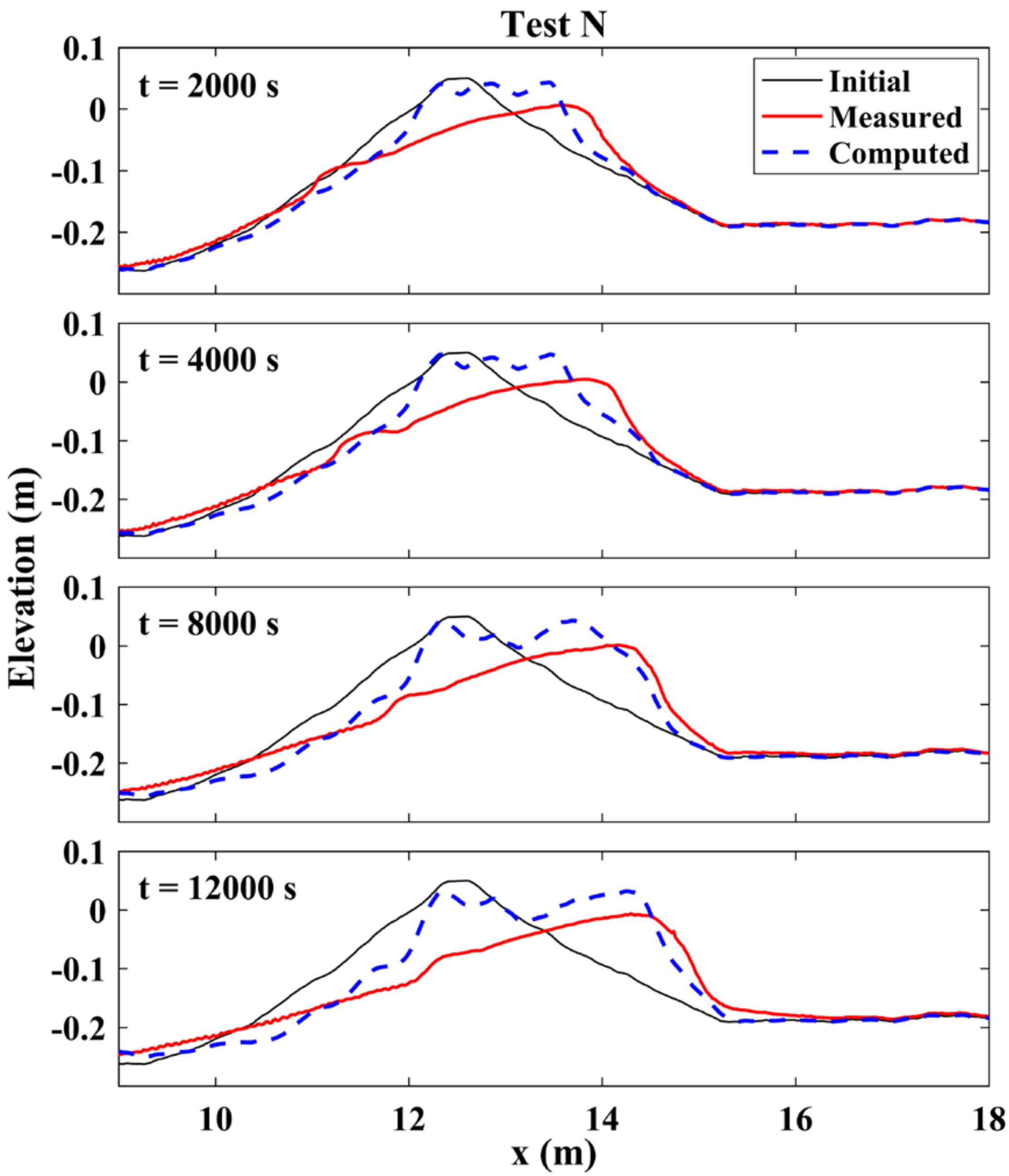

Figure 5.10 Measured and computed profiles at time t = 2,000, 4,000, 8,000, and 12,000 s along with initial profile of Test N

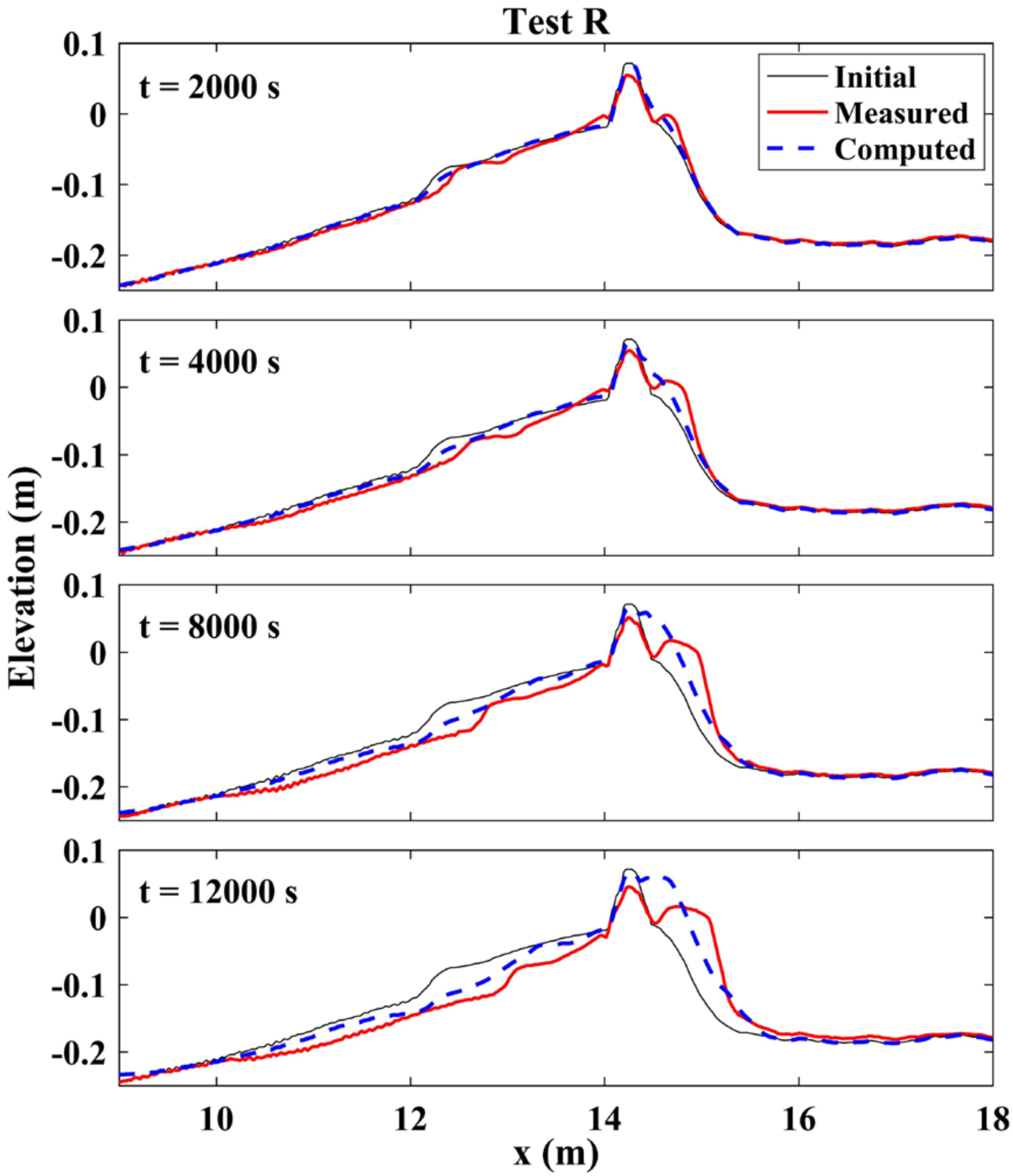

Figure 5.11 Measured and computed profiles at time t = 2,000, 4,000, 8,000, and 12,000 s along with initial profile of Test R

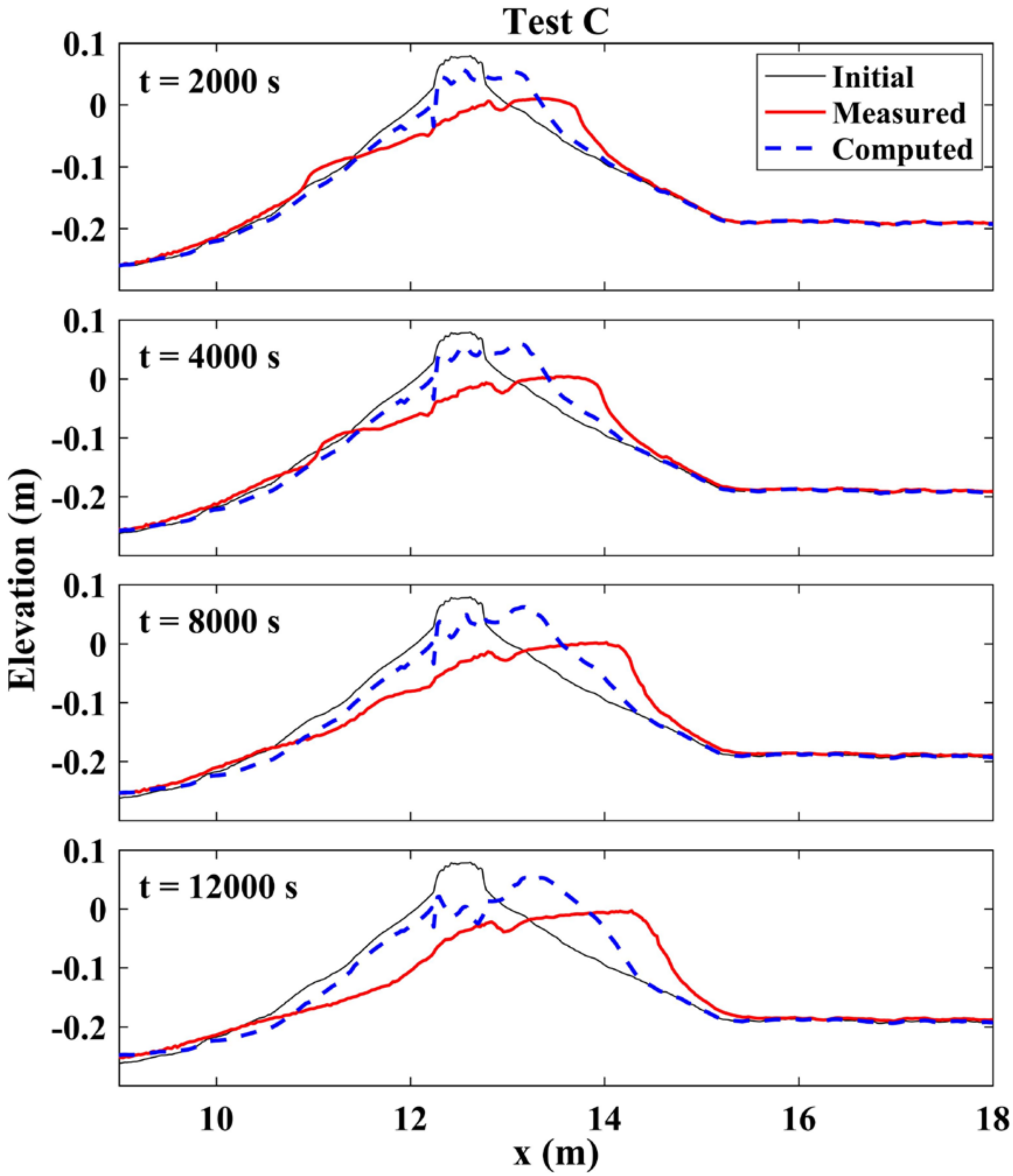

Figure 5.12 Measured and computed profiles at time t = 2,000, 4,000, 8,000, and 12,000 s along with initial profile of Test C

The bed load parameter B and the suspended load parameter a_o were calibrated to reproduce the measured barrier profile evolution in Tests N, R, and C. The standard value of B = 0.002 was calibrated using the field data of 16 beach profiles at Rehoboth and Dewey beaches (Kobayashi and Jung 2012) and applied in previous laboratory experiments (e.g., Yuksel and Kobayashi 2020). The calibrated value of B = 0.01 in this experiment was obtained by comparing the temporal variations of the computed and measured values of V_e as shown in Figure 5.13. The fivefold increase of B increased the onshore bed load transport rate and corresponding eroded sand volume V_e per unit width. The parameter a_o relating to wave overtopping affected the barrier crest profile more than the eroded volume V_e. The calibrated range of a_o was 1.0 – 2.0 for Tests N, R, and C. The computed values of V_e were not very sensitive to the value of a_o. The eroded volume was predicted within errors of about 20% by using the combination of B = 0.01 and a_o = 1.8.

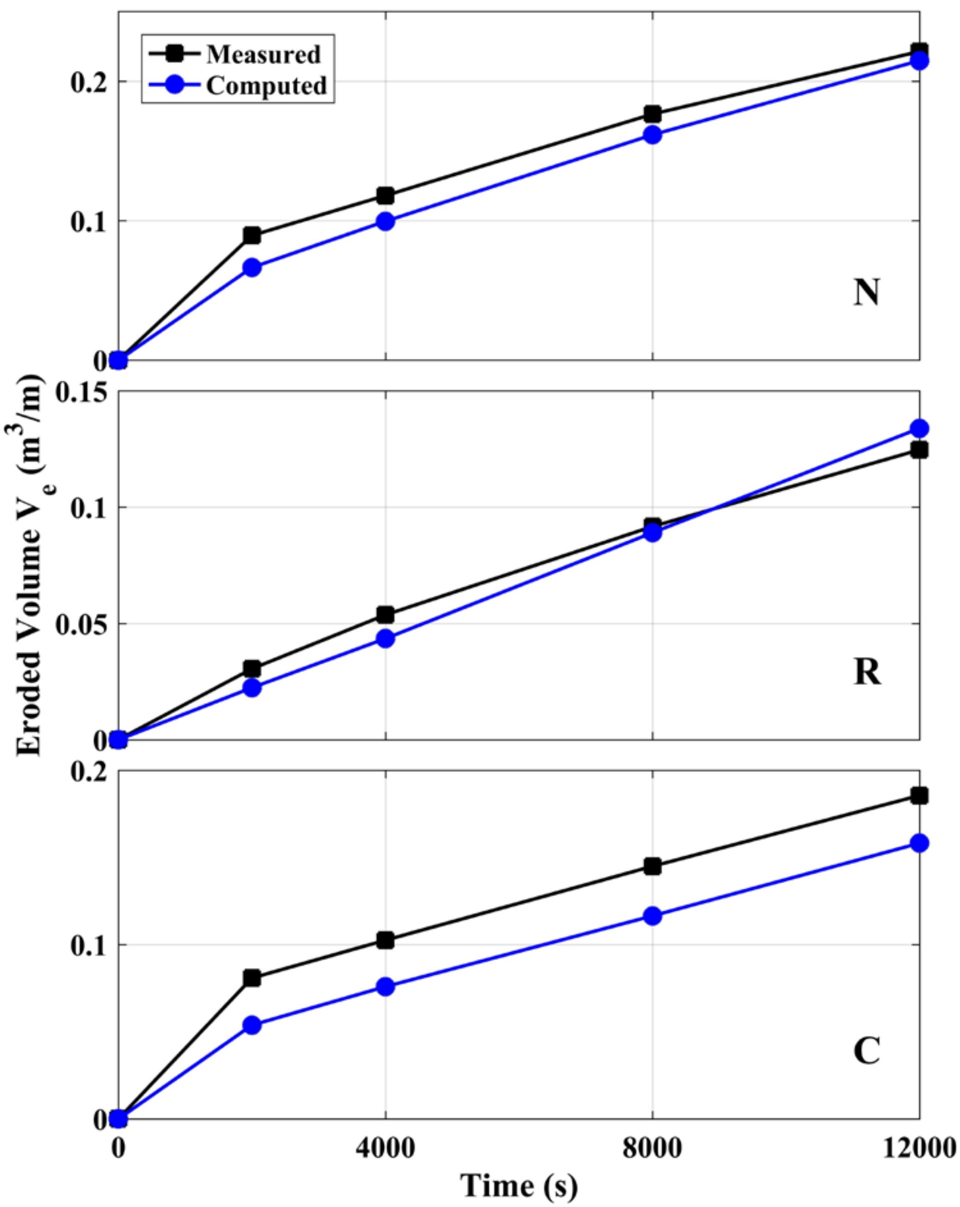

Figure 5.13 Measured and computed eroded volumes V_e per unit width at time t = 2,000, 4,000, 8,000, and 12,000 s for Tests N, R, and C

5.3 Cross-shore Sediment Transport

The computed cross-shore sediment transport rate and cumulative transport volume per unit width at t = 2,000, 4,000, 8,000, and 12,000 s for Tests N, R, and C are plotted in Figures 5.14 – 5.16. The net cross-shore transport rate q_x is the sum of the bed load q_{bx} and suspend load q_{sx} transport rates. The computed cross-shore bed load and suspended load transport rates per unit width are integrated for the given duration (2,000 – 12,000 s) to obtain the cumulative bed load volume v_{bx}, suspended load volume v_{sx}, and net volume $v_x = (v_{bx} + v_{sx})$ per unit width. The cross-shore bed load transport is positive (onshore). The cross-shore suspended load transport is negative (offshore) due to offshore return (undertow) current seaward of the zone dominated by onshore wave overtopping flow and onshore suspended load tranport. Two peaks of the computed bed load and suspended load occurred separately in the vicinity of the barrier crest, expecially for Test N. The net cross-shore sediment transport rate with two peaks produced the computed barrier profile with two peaks in Figure 5.10. The accurate prediction of the barrier profile evolution requires the accurate cross-shore variation of the net sediment transport rate which could not be predicted using constant values of B and a_o.

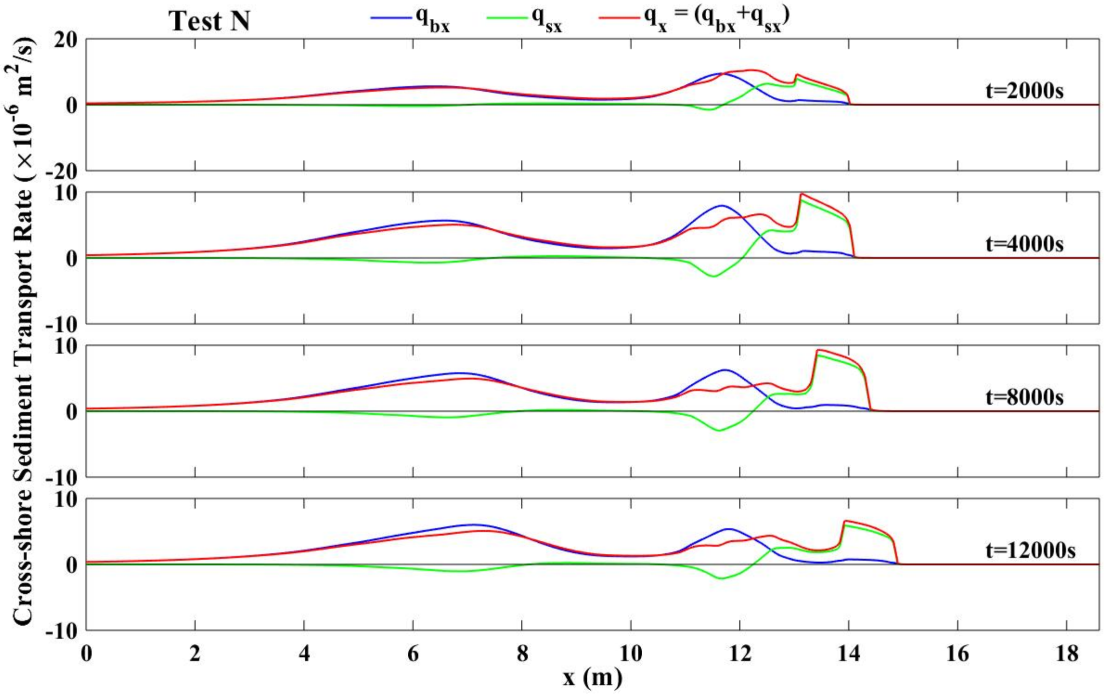

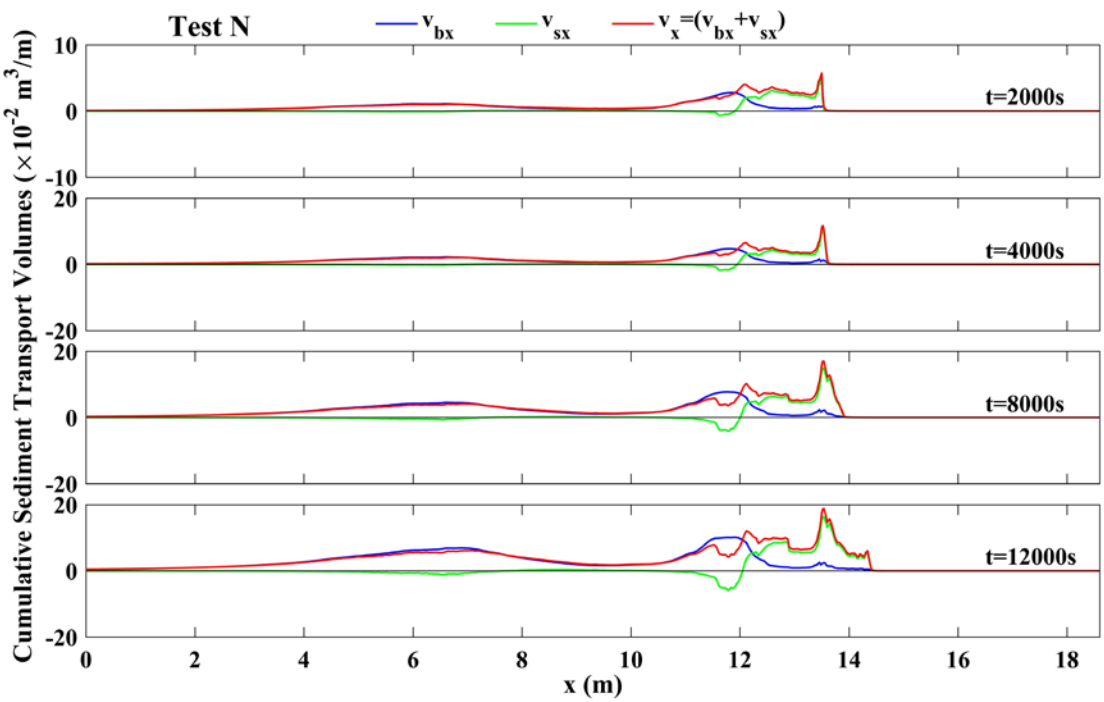

Figure 5.14 Computed cross-shore sediment transport rates and cumulative volumes per unit width at time t = 2,000, 4,000, 8,000, and 12,000 s for Test N

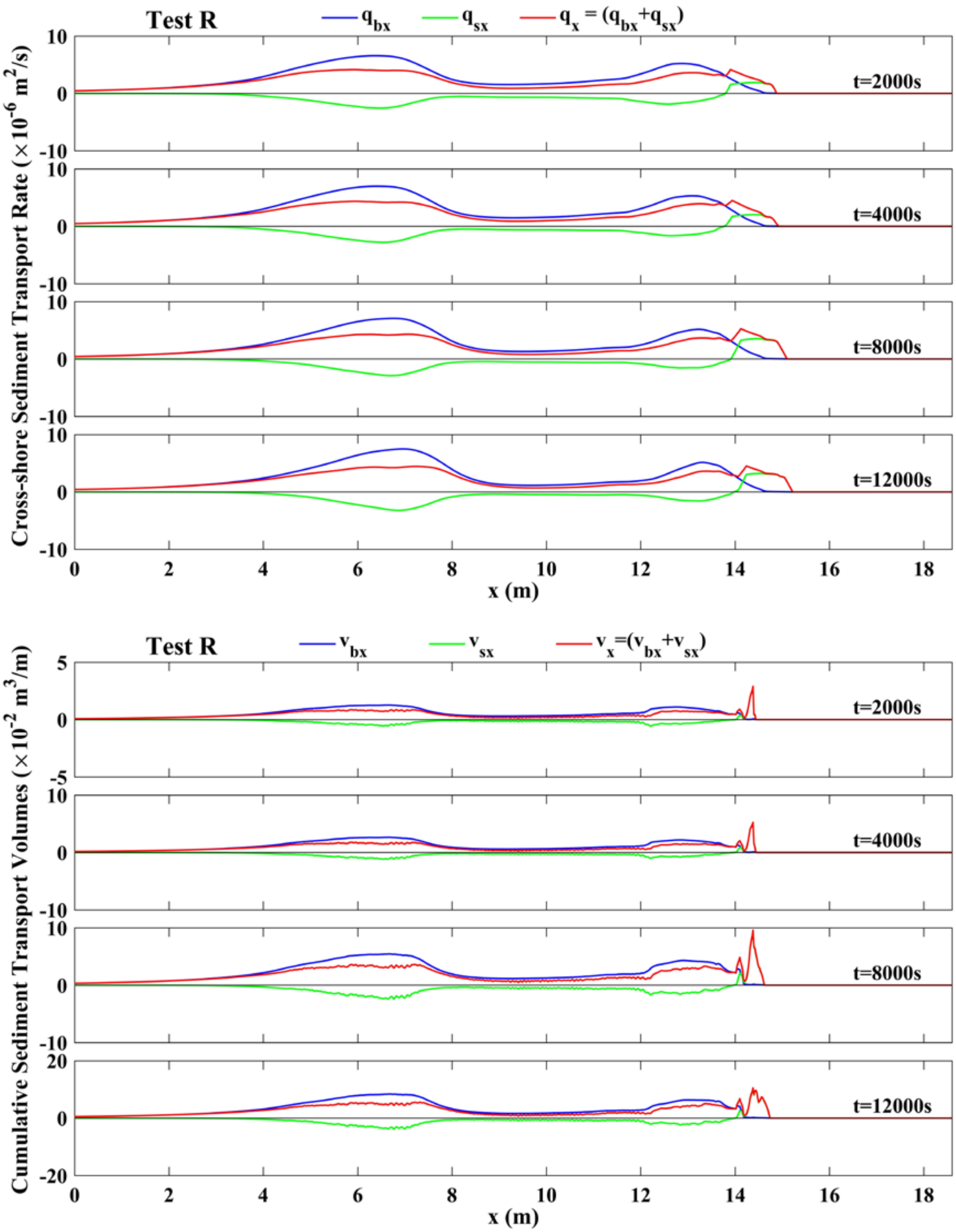

Figure 5.15 Computed cross-shore sediment transport rates and cumulative volumes per unit width at time t = 2,000, 4,000, 8,000, and 12,000 s for Test R

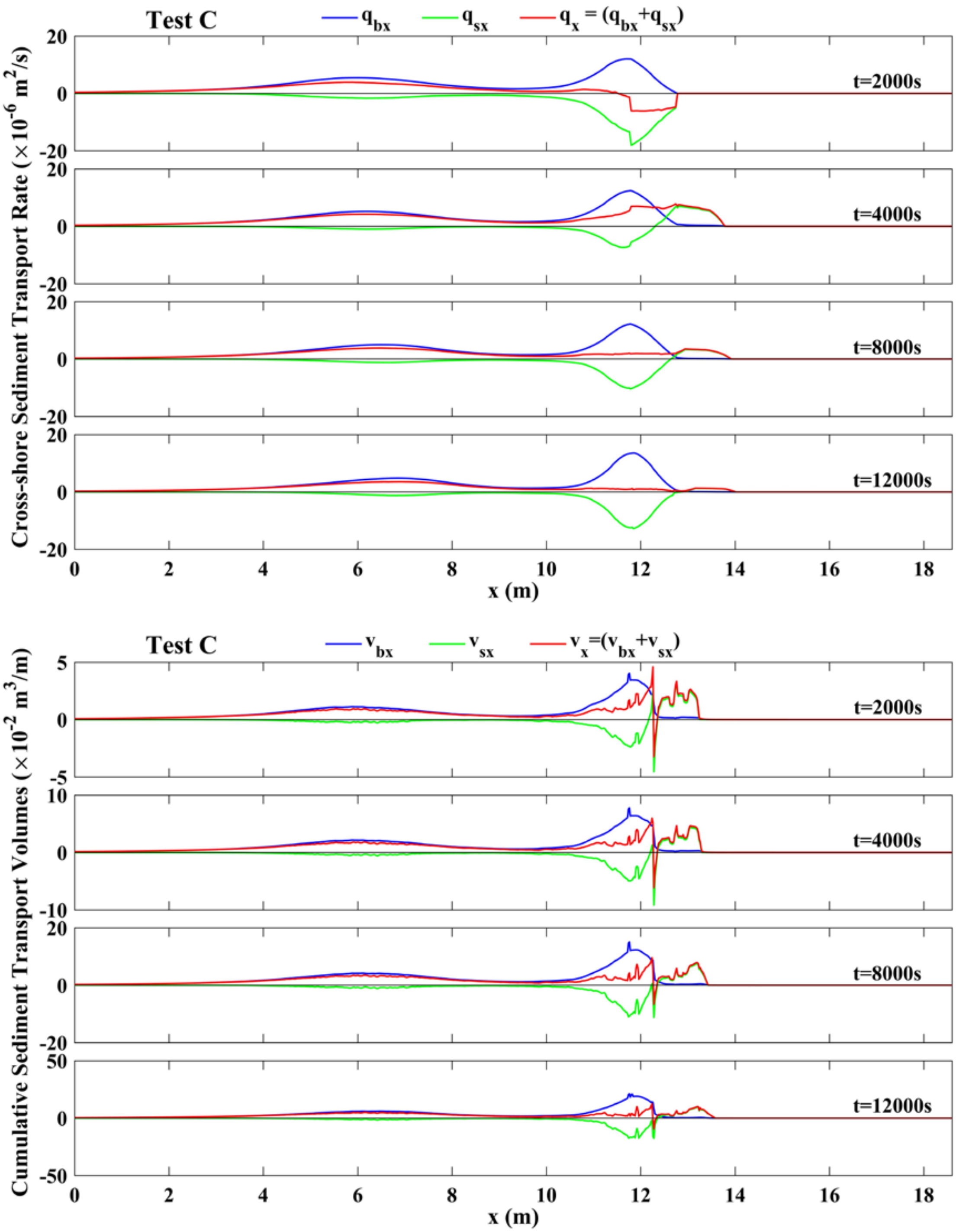

Figure 5.16 Computed cross-shore sediment transport rates and cumulative volumes per unit width at time t = 2,000, 4,000, 8,000, and 12,000 s for Test C

Chapter 6

CONCLUSIONS

6.1 Experimental Findings

Irregular wave overwash and landward migration of a narrow sand barrier was investigated in a laboratory experiment consisting of three tests with each test lasting 12,000 s. The emerged crest of a sand barrier was lowered quite rapidly to the still water level (SWL) at the beginning of Test N with no structure. The sand barrier with its crest near the SWL migrated landward slowly under the same wave condition. The barrier crest became submerged at the end of Test N. A rock mound (Test R) consisting of three layers of stable stones was constructed on the submerged sand barrier in order to reduce its landward migration and crest lowering. The rock mound with no filter settled but its crest remained above the SWL. The landward migration of the sand barrier was reduced only partially in Test R with the rock mound because of onshore sand transport over and through the porous structure. The sand barrier was rebuilt for Test C with a rock cover on the crest of the initial sand barrier of Test N. The rock cover consisting of a single layer of stable stones reduced the sand barrier deformation only slightly because the stone settlement and spreading exposed underlying sand to direct wave action. The intense movement of the exposed sand among the stones could not prevent the sand barrier from landward migration. The design of a rock mound requires the analysis of sand transport over, through, and under the rock mound and the prediction of sand bottom profile evolution.

6.2 Numerical Modeling

The cross-shore model CSHORE was calibrated for a rock structure with no filter and compared with Tests N, R, and C. The mean and standard deviation of the free surface elevation and cross-shore velocity were predicted within errors of about 20% except in the zone of wave transmission (landward of the barrier crest). Small transmitted waves were difficult to predict accurately using the simple hydrodynamic model in CSHORE that may need to be modified in the future. The bed load parameter was increased by a factor of five to reproduce the degree of the profile deformation of the sand barrier without and with the rock mound or cover. The actual profile evolution was predicted marginally because of the difficulty in predicting the cross-shore variation of the sand transport rate. Sand transport processes on the barrier crest and through the porous structure will need to be examined in more detail. Finally, CSHORE will need to be compared with field data (e.g., Gonzalez et al. 2020) in order to demonstrate its utility for practical applications.

REFERENCES

Claudino-Sales, V., Wang, P., and Horwitz, M. H. (2010). "Effect of Hurricane Ivan on coastal dunes of Santa Rosa Barrier Island, Florida: Characterized on the basis of pre- and poststorm LIDAR surveys." J. of Coastal Res., 26(3), 470–484.

Coogan, J. S., Webb, B. M., Smallegan, S. M., and Puleo, J. A. (2019). "Geomorphic changes measured on Dauphin Island, AL, during Hurricane Nate." Shore & Beach, 87(4): 15–22.

Figlus, J., Kobayashi, N., Gralher, C., and Iranzo, V. (2011). "Wave overtopping and overwash of dunes." J. Waterway, Port, Coastal, Ocean Eng., 137(1), 26–33. https://doi.org/10.1061/(ASCE)WW.1943-5460.0000060.

Froede, C. R. (2008). "Changes to Dauphin Island, Alabama, brought about by Hurricane Katrina (August 29, 2005)." J. Coastal Res., 24(4C): 110–117.

Garcia, R., and Kobayashi, N. (2015). "Trunk and head damage on a low-crested breakwater." J. Waterway, Port, Coastal, Ocean Eng., 141(2): 04014037. https://doi.org/10.1061/(ASCE)WW.1943-5460.0000276.

Gonzalez, V.M., Garcia-Moreno, F.A., Melby, J.A., Nadal-Caraballo, N.C., and Godsey, E.S. (2020). "Alabama Barrier Island Restoration Assessment life-cycle structure response modeling." ERDC/CHL TR-20-5. Vicksburg, MS: US Army Engineer Research and Development Center.

Harter, C., and Figlus, J. (2017). “Numerical modeling of the morphodynamic response of a low-lying barrier island beach and foredune system inundated during Hurricane Ike using XBeach and CSHORE.” Coastal Eng., 120, 64–74.

Irish, J. L., Lynett, P. J., Weiss, R., Smallegan, S. M., and Cheng, W. (2013). “Buried relic seawall mitigates Hurricane Sandy’s impacts.” Coastal Eng., 80, 79–82.

Kobayashi, N. (2016). “Coastal sediment transport modeling for engineering applications.” J. Waterway, Port, Coastal, Ocean Eng., 142(6): 03116001. https://doi.org/10.1061/(ASCE)WW.1943-5460.0000347.

Kobayashi, N., and Jung, H. (2012). “Beach erosion and recovery.” J. Waterway, Port, Coastal, Ocean Eng., 138(6), 473–483. https://doi.org/10.1061/(ASCE)WW.1943-5460.0000147.

Kobayashi, N., and Kim, H. D. (2017). “Rock seawall in the swash zone to reduce wave overtopping and overwash of a sand beach.” J. Waterway, Port, Coastal, Ocean Eng., 143(6), 04017033. https://doi.org/10.1061 /(ASCE)WW.1943-5460.0000416.

Kobayashi, N., Pietropaolo, J., and Melby, J. A. (2013). “Deformation of reef breakwaters and wave transmission.” J. Waterway, Port, Coastal, Ocean Eng., 139(4), 336–340. https://doi.org/10.1061/(ASCE)WW .1943-5460.0000180.

Kobayashi, N., and Zhu, T. (2017). “Bay flooding through tidal inlet and by wave overtopping of barrier beach.” J. Waterway, Port, Coastal, Ocean Eng., 143(5): 04017024. https://doi.org/10.1061/(ASCE)WW.1943-5460.0000403.

Smallegan, S. M., and Irish, J. L. (2017). “Barrier island morphological change by bay-side storm surge.” J. Waterway, Port, Coastal, Ocean Eng., 143(5): 04017025. https://doi.org/10.1061/(ASCE)WW.1943-5460.0000413.

Strazzella, M., Kobayashi, N., and Zhu, T. (2019). “Analysis and prediction of storm water levels in Delaware inland bays.” Shore & Beach, 87(2): 29–35.

Webb, B. M., Douglass, S. L., Dixon, C. R., and Buhring, B. 2011. “Coast guards.” Civil Engineering, ASCE, December 2011, 76–83.

Yuksel, Z. T., and Kobayashi, N. (2020). “Comparison of revetment and sill in reducing shore erosion and wave overtopping.” J. Waterway, Port, Coastal, Ocean Eng., 146(1): 04019028. https://doi.org/10.1061/(ASCE)WW.1943-5460.0000543.